EXTENSION OF DYNAMIC OPERATIONAL RANGE IN ALKALINE WATER ELECTROLYSIS PROCESS

Lappeenranta-Lahti University of Technology LUT

Master's Programme in Chemical Engineering

Master's Thesis 2024

Shiva Gandu

Examiners: Docent Arto Laari

Assistant Professor Nima Rezaei

ABSTRACT

Lappeenranta–Lahti University of Technology LUT

LUT School of Engineering Sciences

Master's degree Programme in Chemical Engineering

Shiva Gandu

Extension of dynamic operational range in alkaline water electrolysis process

Master's thesis

2024

64 pages, 29 figures, and 04 tables

Examiners: Docent Arto Laari

Assistant professor Nima Rezaei

Keywords: Alkaline water electrolysis, gas crossover, hydrogen, oxygen, recirculation, and diffusion.

Currently, hydrogen is predominantly produced through the reforming of fossil fuels which emits the greenhouse gases failing to meet carbon reduction requirements. In contrast water electrolysis, a simpler technology that produce hydrogen with 99.9% purity. Long term energy storage, through energy-rich hydrogen, is considered promising as it allows for the use of surplus renewable energy generated during period of low demands. Water electrolysis, particularly alkaline water electrolysis has been applied in the industry for decades and is often discussed as a key technology for future hydrogen synthesis due to its fast dynamic response varying operating conditions. Renewable-powered alkaline electrolysis has the potential to play critical role in the transition to a low-carbon energy future. However, in this integration the variability in renewable energy supply can lead to frequent start-stop cycles and fluctuating operational conditions for electrolysis affecting their efficiency and longevity. Advanced control systems, integrating energy storage and dynamic load management can address these challenges.

This paper examines the extension of the dynamic operating range in alkaline water with respect to product gas purity. Specifically, it analyzes the gas crossover in product gases due to the dissolution of gas molecules in circulating electrolyte solution and diffusion through diaphragm and suggests methods to reduce it, including decreasing the pressure in the oxygen separator, controlling electrolyte circulation rate, and removing dissolved gases from the electrolyte. The study investigates variations in electrolyte flow rate (kg/h), capacity (MW) and gas composition (%). Simulation ware conducted in Aspen Plus using a 30 wt% KOH alkaline electrolyte solution at 80 ^{o}C and 16 bars pressure. The result indicates that for wide range operation of the plant and safe process shutdown, removing dissolved gases through the membrane wall in gas-liquid membrane module significantly affect gas composition, ensuring impurities remains below safety levels even when the load drops to 10% of maximum capacity.

Moreover, control of the electrolyte circulation rate at low power inputs helps to keep gas composition at constant level reducing gas crossover.

ACKNOWLEDGEMENTS

This master's thesis was carried out at Lappeenranta-Lahti University of Technology (LUT) in Lappeenranta.

I would like to extend my gratitude to Docent Arto Laari being my mentor throughout this project. His inputs and guidance were so valuable. He is there in every hardship, especially when things became more complicated. He made things so simple, so that understand and perform well. I'm also so grateful to Nima Rezaei, Hung Nguyen and Vesa Ruuskanen.

A special heartfelt thanks goes to my friends in chemical engineering, with whom I have shared my views to put this project on better place. I also have both good and bad memorable moments with them. I also thank all my professors who taught chemical engineering subjects and made me part of numerous group projects which helped me to use all my knowledge in this project.

Finally, I want to express my deepest gratitude to my family and friends for their unaccountable and continuous support during my thesis and throughout my studies.

Symbols and abbreviations

Roman characters

A	Area, m^2
C	Concentration, mol L^{-1}
C_p	Heat capacity J K^{-1}
C_s	Gas solubility, mol L^{-1}
C_t	Thermal capacitance, J K^{-1}
D	Diffusion coefficient, m^2 s^{-1}
E	Observed electrode potential, J
E_c	Total number of cells
F	Faraday constant, C mol^{-1}
h_i	Salt, specific constant, mol^2 L^{-2}
h_{Gi}	Gas specific constant, J mol^{-1} K^{-1}
I	Current, A
i	Current density, A m^{-2}
K	Reaction quotient
l	Length, m
$\dot{m}$	Mass flow rate, kg h^{-1}
N	Diffusion rate, kg h^{-1} m^{-2}
$\dot{n}$	Molar flow rate, mol h^{-1}
n_s	Gas separation efficiency
n_{sl}	Liquid separation efficiency
P	Pressure, bar
Q	Heat, J
R	Resistance, ohm(Ω)
T	Temperature, K, ^oC

V	Voltage, V
U	Potential energy, J

Greek symbols

α	Electrode's charge transfer coefficient
δ_{sep}	Thickness of the separator, m
ρ	Density, kg/m^3
τ	Tortuosity
ε	Porosity of the separator
Θ	Fractional bubble coverage on the electrode surface

Subscript

an	Anode
act	Activation
amb	Ambient
cat	Cathode
cool	Cooling
e	Electrode
eff	Effective
el	Electrolyte resistance
gen	Generation
H_2	Hydrogen
H_2O	Water
O_2	Oxygen
i	Inlet
j	Outlet
liq	Liquid

ohm	Ohmic
oc	Open circuit
rev	Reversible
sat	Saturation
sep	Separator
stack	Electrolysis stack
up	Upward gas-liquid separator outlet
vap	Vapor

Abbreviations

AWE	Alkaline Water Electrolysis
ACM	Aspen Custom Modeler
CGEP	Center on Global Energy Policy
ENRTL-RK	Electrolyte Non-Random Two-Liquid - Redlich-Kwong
HER	Hydrogen Evolution Reaction
HTEL	High Temperature Electrolysis
HTO	Hydrogen Volume Fraction in Oxygen
OER	Oxygen Evolution Reaction
OTH	Oxygen in Hydrogen
PEMWE	Proton Exchange Membrane Water Electrolysis
PEML	Polymer Electrolyte Membrane Electrolysis
PPS	Polyphenylene Sulfide
RES	Renewable Energy Sources
SOEC	Solid Oxide Electrolytic Cell
SOEL	Solid Oxide Water Electrolysis
UTP	Ultra-Thin PTFE
VPS	Vacuum Plasma Spraying

Contents

1. Introduction

1.1. Background

The continuous growth of renewable energy sources, such solar and wind power, calls for storage and regulatory systems to provide a steady and reliable energy supply (Parra et al., 2016). This need arises from the inherently variable nature of these energy sources. For short-term energy storage needs, technologies like batteries and supercapacitors prove to be efficient (Díaz-González et al., 2012). Nonetheless, chemical carriers such as synthetic natural gas or hydrogen are sometimes seen to be more practical choices for long-term storage.

By combining a water electrolyser and a renewable energy source, a power-to-gas facility can produce hydrogen, an essential energy carrier (Ursua et al., 2016). Excess renewable energy can be converted through this process into hydrogen, which has multiple applications. It can be used as a raw material to make other chemicals like methane or ammonia, or it can be fed into the current natural gas distribution and storage system to be transformed back into power using fuel cells. This approach not only aids in balancing the energy grid but also opens pathways for renewable energy utilization in sectors beyond electricity (Momirlan and Veziroglu, 2005).

AWE is the developed and widely used electrolysis method among the various possibilities available. In AWE, the process involves electrodes that are submerged in a solution of KOH, typically ranging from 20% to 40% by weight. A diaphragm is used to stop the H_2 and O_2 gases produced at the cathode and anode, respectively, from mixing. This separator is crucial as it allows the passage of ions necessary for the electrolysis reaction while physically keeping the evolved gases separate, so guaranteeing the quality of the O_2 and H_2 generated (Carmo et al., 2013). A gradient in the concentration of electrolyte is produced in a stack due to the asymmetric generation and consumption of water in the half-cells. The electrolyte solutions in the electrode cycles are continuously blended in order to balance this disparity. However, this mixing strategy constrains the operational range to approximately 10% to 40% of the nominal capacity because oxygen purity significantly diminishes when hydrogen contamination occurs below this threshold according to Ursua et al., (2013). The gas-saturated electrolyte solution's mixing and hydrogen passage across the separator allow dissolved species to move to the other

gas separator, causing contamination. As a result, industrial electrolysers are typically shut down when the concentration of a foreign gas, such as hydrogen, reaches 2% by volume in the exhaust (Schalenbach et al., 2013), which is about half the explosive threshold for hydrogen-oxygen mixture (Schröder et al., 2004). This safety measure becomes particularly critical when the electrolyser operates with RES minimal current densities (Hug et al., 1992).

1.2. Objectives

Certain flexibility in electrolysis technology is required due to the unpredictability of the current supply; this is especially true for alkaline electrolysers. The lowest current density required for safe operation, or the minimum operational load, usually falls between 10% and 40%. The hydrogen volume fraction in oxygen (HTO) plays a major role in determining this minimum level. A vital threshold of 2% HTO is set to prevent explosive combinations, which prompts the development of a 1.6% HTO alert value to prevent repeated emergency shutdowns (Cheng et al., 2024). Factors such as diaphragm properties, solubility of gases in electrolyte, operating conditions, and current density influence HTO levels. With lower current densities increasing the likelihood of higher HTO due to reduced hydrogen and oxygen production rates (Trinke et al., 2018).

Optimizing alkaline electrolysis involves determining ideal operating conditions, study conducted by Leng et al., (2012) indicating potential improvements through reduced diaphragm thickness. However, such analyses are constrained by little experimental data to validate models, particularly concerning current-voltage curves and gas crossover. Most existing studies provide data for a single set of conditions, often at atmospheric pressure and temperature, with few investigations into how temperature and pressure affect performance, especially for less efficient alkaline electrolysers. Recent research by Sakas et al., (2022) and Haug et al., (2017) has begun to address the gap in data on hydrogen gas crossover, highlighting the need for further experimental validation to optimize alkaline electrolysis technology fully.

In this work an Aspen Plus model is developed and used to validate the performance of AWE. The model concentrates on the evolution of gas purity considering the effect of electrolyte concentration, electrolyte circulation rate, current density, and range of power input on the performance of electrolysis stack for H_2 production efficiency and purity of product gases which is limited by accumulation and mixing of gases. The operating conditions of an industrial

electrolyser proposed by Sakas et al., (2022) are used to evaluate the model. Then, the electrolyte flow rate, current density, electrolyte concentration and current density are varied systematically and analyzed regarding the resulting gas purity to derive possible safe operating conditions. The developed aspen model can be used to evaluate safe operating range at different conditions, especially when power load changes duo to variability in renewable power availability. It can also be used to test different scenarios and to invent and test methods to improve and extend the operational range. It is also benefit that it uses built-in thermodynamic models to evaluate gas solubilities and vapor pressures essential in process simulations.

2. Water electrolysis

Water electrolysis is the breaking of water molecules in to H_2 and O_2 molecules with an electric current. This process essential for producing H_2 which has the potential to be clean, sustainable energy source. Water electrolysis is fueled by electrical energy. In this process, hydrogen which is positively charge ions are drawn to the cathode, which is negatively charged by the electric current, where they undergo a reduction reaction to produce hydrogen atoms. Gaseous hydrogen molecules are created when these hydrogen atoms combine (H_2). Conversely, oxygen was created at the positively charged anode seen in the Figure 1.

$$Cathode: 2H_2O(l) + 2e^- \rightarrow H_2(g) + 2OH^-(aq) \quad (1)$$

$$Anode: 4OH^-(aq) \rightarrow O_2(g) + 2H_2O(l) + 4e^- \quad (2)$$

$$Overall\ Reaction: 2H_2O(l) \rightarrow H_2(g) + O_2(g) \quad (3)$$

In the construction of electrolysis unit, the most important things that need to be taken care of are adequate use of electrodes to increase the efficiency of energy, improved production rates and to avoid unwanted reactions to improve the purity of hydrogen.

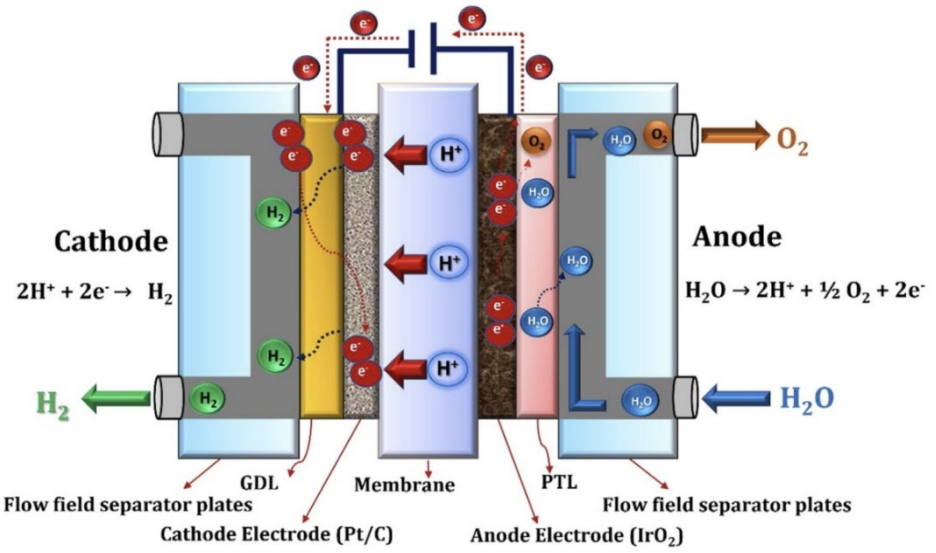

Figure 1 Electrolysis Cell with H^+ proton permeable membrane (Paidar et al., 2016)

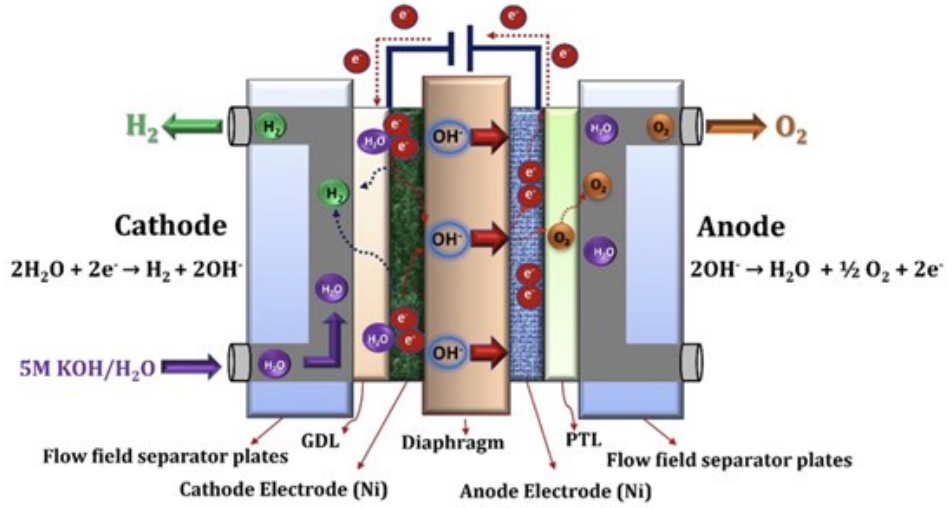

Figure 2 Electrolysis Cell with OH^- permeable diaphragm membrane (Paidar et al., 2016)

Ions, protons, electrons, and oxygen or hydrogen atoms can pass through a chosen separating membrane in the

Figure 2 the electrolysis process's overall economics, performance, and efficiency are all directly impacted by this choice. Some important factors in membrane selectivity are the ion selectivity, stability, conductivity, gas crossover, cost, and compatibility with the electrolyte.

Alkaline water electrolysis (AWE), polymer electrolyte membrane electrolysis (PEML), and solid oxide water electrolysis (SOEL) are the three primary forms of water electrolysis (SOEL

which is at this moment still under the developing stage). In order to keep the product gas from mixing during alkaline electrolysis, a gas-impermeable separator is needed. The KOH or NaOH which are concentrated are used in the electrolyte. Metals such as nickel which are said to be non-noble, with an electrolytic on it make up the electrodes. The metals platinum and iridium are used to be electrocatalysts in PEMEL are the noble metals. Along with polymer membrane which is humidified serving as the electrolyte. Both systems support pressures maximum 30 bar and operate in the 50–80 °C temperature range. Both approaches have a notional stack efficiency of about 70% (Carmo et al., 2013). SOEL is also said to be HTEL due to it is operated at high temperatures between 700 and 900 ºC. SOEL thermodynamic influences on power usage at higher temperatures theoretically allow efficiencies of stack near to 100%. For economical operation, however, the increased thermal demands necessitate the use of a waste heat source from the thermal power generation, metallurgical, or chemical industries. Furthermore, SOEL only offers small stack capacities under 10 kW, whereas AWE and PEMEL offer 6 MW and 2 MW, respectively (Buttler et al., 2018). Therefore, the cost of investment and lifetime for AEL or PEMEL is the favorable system design for large-scale production (Brauns and Turek, 2020).

Researchers have focused on predicting the power needed and hydrogen output of alkaline electrolysers. Ulleberg, (2003) developed a model that estimates cell voltage, which has been widely adopted. Other studies, like (Haug et al., 2017) and (Zarghami et al., 2020), looked at gas purity and motion of gases inside the electrolyser. Dynamic models, like the one by David et al., (2020), helps to understand how gas production can be controlled. Sánchez et al., (2018) used a model to understand energy losses and polarization across different conditions.

2.1. Alkaline water electrolysis

One of the earliest and most well-known techniques for electrolyzing water is alkaline electrolysis. With the help of KOH or NaOH water can split into H_2 and O_2 gases in AE. First suggested in 1789, AE was first used on an industrial basis in 1939, with a power output of roughly 50 MW. Lower temperatures (30–80 °C) are used for alkaline water electrolysis, which uses concentrated alkaline solutions (5 M KOH/NaOH). These systems use asbestos/PPS/composite ZrO_2 separators and nickel-coated stainless-steel electrodes. Hydroxide ions (OH^-) are the ionic charge carriers; water and KOH/NaOH pass through the separator to facilitate electrochemical processes. Benefits include inexpensive materials, and

high effectiveness at greater sizes, Alkaline electrolyzes are proven to have extended operational lifetimes, ranging from 3.5 to 11.5 years (CGEP, 2024). AWE schematic is shown in the Figure 3.

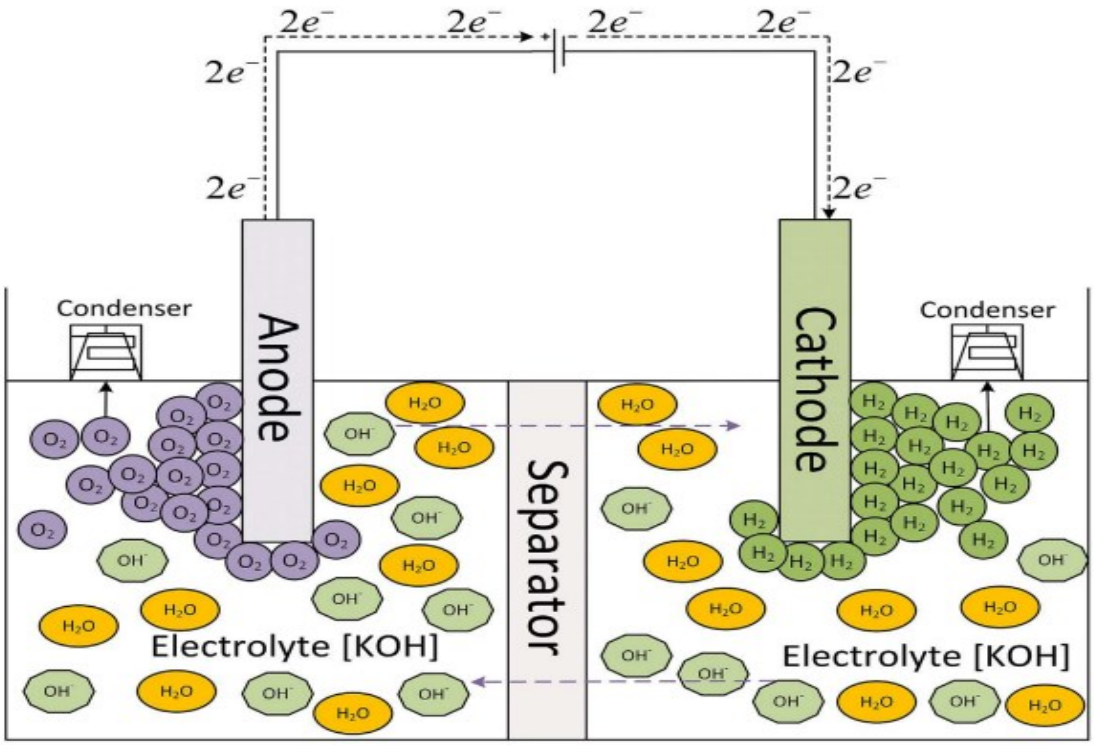

Figure 3 Schematic of the alkaline electrolysis cell (Abdin et al., 2017)

2.2. PEM water electrolysis

The membranes which are acidic are used in PEMWE as solid electrolytes due to pure water partially self-ionizes. The fundamental components of a PEMWE cell are bipolar plates, gas diffusion layers, and a membrane covered with a catalyst as in the Figure 4. The solid acidic membrane that divides the two half-cells supports the cathode and anode catalyst layers, transports protons, and separates product gases. The catalyst layers offers high mass transport channels for water and product gases when they are compressed between gas diffusion layers which are porous these coated catalyst carry heat and electrons between the bipolar plates and layers of catalyst. At this point of process water is breaks into protons and electrons and molecular oxygen when water is added to anode. Protons have the potential to go across the

membrane towards cathode, where they can be converted to molecules of hydrogen when they generated at anode. (Feng et al., 2017).

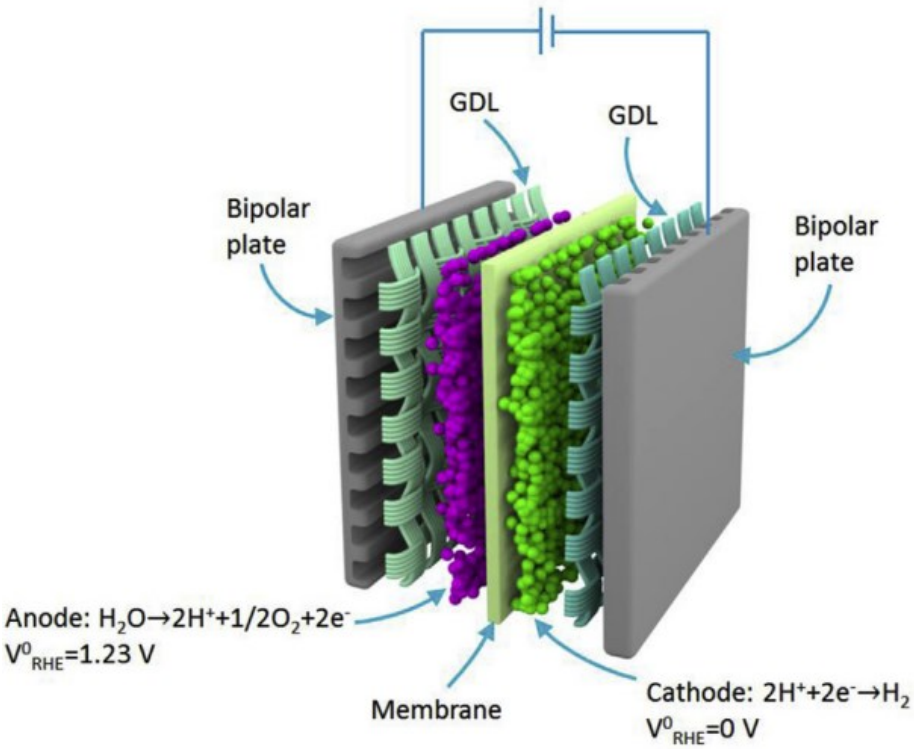

Figure 4 Schematic cross-section of a PEM electrolyser (Feng et al., 2017)

$$Anode: 2H_2O \leftrightarrow O_2 + 4H + + 4e^- \quad (4)$$

$$Cathode: 4H + + 4e^- \leftrightarrow 2H_2 \quad (5)$$

The metals platinum (Pt) and palladium (Pd) are electrocatalyst for HER at the cathode and at anode RuO_2/IrO_2 for the OER are widely used in the field of PEM electrolysis (Xu and Scott, 2010). The study at General Electric demonstrated the effectiveness of these systems, obtaining an impressive operational longevity of 15000 hours without seeing any degradation in performance (Rozain and Millet, 2014). The exorbitant cost of these precious minerals limits the application of PEM electrolysis, despite its obvious benefits such as high current densities and superior gas purity.

2.3. Solid oxide electrolyte cell water electrolysis

The two porous electrodes, the anode and cathode, and the ionic conducting electrolyte are essential parts of the solid oxide electrolytic cell construction (SOEC) seen in the Figure 5. The electrolyte cells receive the necessary electrical energy when steam is supplied to the cathode. Consequently, at the reaction sites, the water molecules diffuse to the cathode-electrolyte interface where they breakdown to produce H_2 gas and oxygen ions. As it pass to the cathode area, the generated hydrogen gas gathers. At the anode, the O_2 ions are transferred and oxidized to produce O_2. The energy of both electrical and thermal significantly reduced with an increase in temperature. Consequently, high-temperature SOEC is beneficial since it offers more chances to use waste heat for the creation of hydrogen (Meng et al., 2008).

$$Anode: 2O^{2^-} \leftrightarrow O_2 + 4e^- \quad (6)$$

$$Cathode: 2H_2O + 4e^- \leftrightarrow 2H_2 + 2O^{2^-} \quad (7)$$

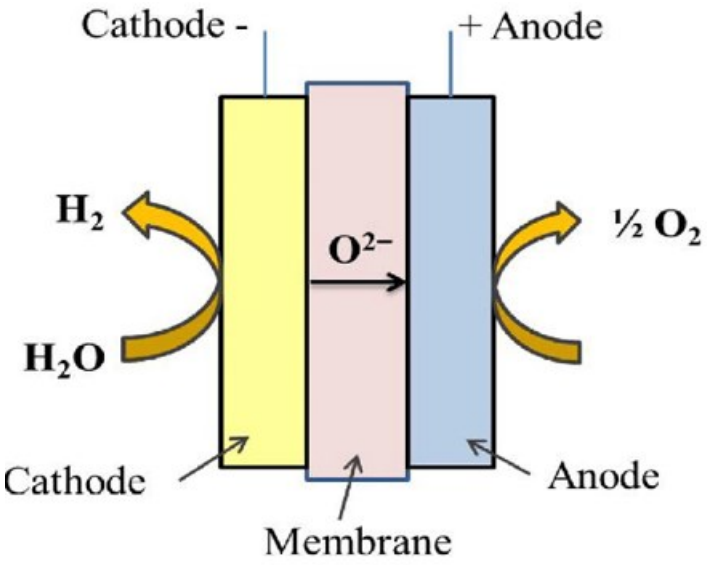

Figure 5 A illustration of the SOEL (Shiva Kumar and Himabindu, 2019)

3. Alkaline electrolysis process

3.1. Alkaline water electrolysis process structure and components

Manabe et al., (2016) reported that to ensure optimal performance and longevity of the cell or electrolyser, careful consideration of the cell design is essential. Four key factors contribute to enhancing cell performance: the anode, cathode, separator, and electrolyte concentration. In this investigation, particular attention was directed towards the electrolyser, leading to the elucidation of the following points:

3.1.1. Electrodes and catalysts

Nickel, renowned for its robust activity, wide availability, and cost-effectiveness, stands out as a favored electrode material for alkaline electrolysis (Janjua and LeRoy, 1985). For water electrolysis to produce H_2 more efficiently, an electrocatalyst must be used since it diverts reaction routes away from higher activation energies. The activity of the electrocatalyst have a major role in the efficiency of the OER and the HER. Activated electrodes and other combinations of metals and oxides can be enhanced by adding cobalt or molybdenum to the alloy, using vacuum plasma spraying (VPS) to apply combination of alloy onto the electrode or applying galvanic deposition of these alloys. Transition metal-based cathode materials have shown noticeably higher electrocatalytic activity than traditional electrodes. Ruthenium oxide (RuO_2), spinel-type oxides (Co_3O_4), perovskite-type oxides $LaCoO_3$, and $LaNiO_3$ are just a few of the many mixed oxides that have been investigated to minimize anode overpotential. All of these oxides function as electrodes, display catalyst qualities, and drastically lower potential requirements (Smolinka et al., 2011).

Molecular electrocatalysts like $BIMBF_4$ $[Ni(P_2N_2)_2](BF_4)_2$ and combinations of ionic liquid solutions with different electrodes have been extensively studied, optimized and tested in lab level (Souza et al., 2007).

3.1.2. Separator

In an electrochemical cell, the separator serves two purposes. First, it prevents electrode short circuits and prevents hydrogen and oxygen gases from combining. It must therefore continue to be stable in the frequently severe alkaline environment that characterizes its electrolyzes. To minimize voltage drops, it should also have better conductivity to facilitate the flow of OH^- ions between the anode and cathode. This conductivity is closely related to the porosity and tortuosity of the separator, which controls the current flow via the liquid electrolyte contained in its pores (Peng, 2023). Diaphragms, utilized for the separation between the anode and cathode, employ various materials. Asbestos was used as Diaphragms in earlier processes. However, due to health and safety regulations, asbestos is no longer utilized. Alternately, Zifron separator is widely used. The study conducted by Brauns et al., (2021) compared Zirfon$_{TM}$ Perl UTP 500 with pre-commercial diaphragms in alkaline water electrolysis. Thinner Zirfon diaphragms exhibited lower ohmic resistances but increased gas impurity, favoring higher current densities. Thicker diaphragms may be preferable for lower current densities or high gas purity.

3.1.3. Electrolyte solution

The conducting medium for the electrolysis process is the electrolyte solution, which normally consists of water and a soluble base like KOH or NaOH. This solution prevents considerable corrosion losses that are associated with acidic electrolytes in addition to facilitating electrical conduction (LeRoy, 1983). To enhance the solution's conductivity, electrolytes containing ions with high mobility are utilized.

According to published research, KOH solutions reach their optimum conductivity at 80°C at about 35 weight percent (Hine, 1985). But depending on the kind of separator, different alkaline water electrolysis (AWE) plants have different ideal KOH concentrations. Analyte flow rate experiments showed that in the zero-gap AWE system, the electrolyte flow rate within the cell had no discernible effect on hydrogen purity (Phillips et al., 2016). Approximately 2.94 kPa differential pressure operation, a steady catholyte flow from cathode to anode side through the diaphragm is assumed, facilitating the transfer of both dissolved and generated H_2 gas to the anode side.

3.2. Industrial alkaline electrolysis process

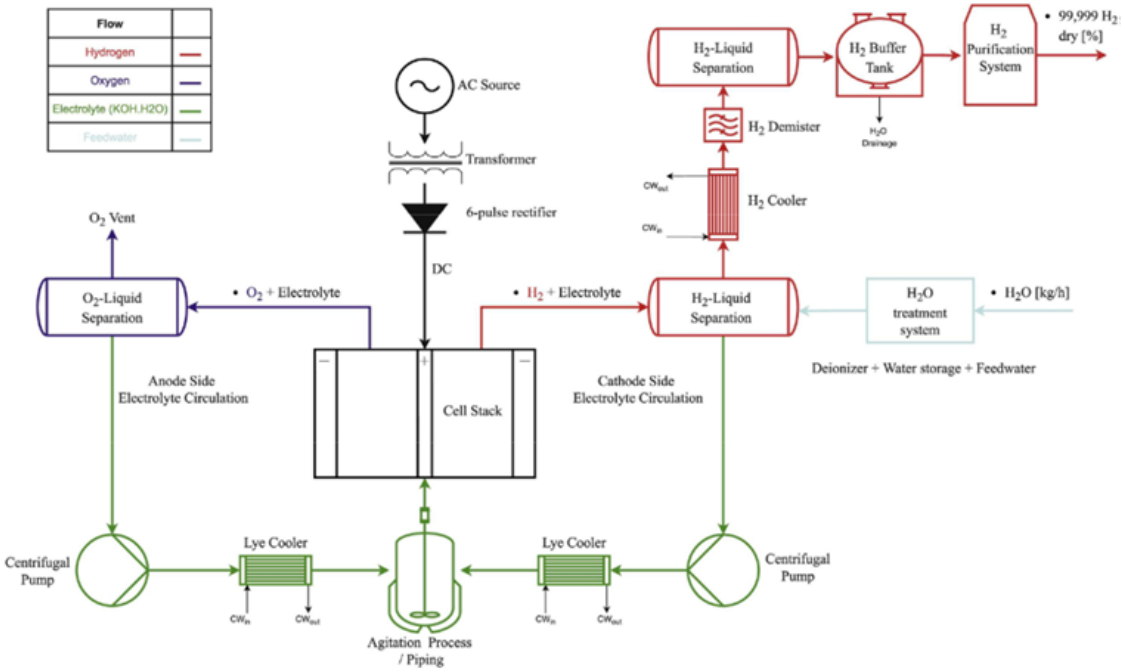

Figure 6 process flow diagram of an alkaline electrolyser plant (Sakas et al., 2022)

Sakas et al., (2022) used an AC electric current, which is transformed into DC by a 6-pulse thyristor rectifier following transmission from a transformer (Figure 6). This DC current, along with AC ripple, is supplied to an electrolyser cell stack. Here, water is electrolyzed into H_2 and O_2 using electrodes and a potassium hydroxide (KOH) solution ranging from 20% to 30% concentration (O'Hayre et al., 2016). The resulting gas-electrolyte mixture is then divided into separate streams through separators (Towler and Sinnott, 2021). These separators are interconnected by an equalization tube to maintain balance in mass and energy.

The electrolyte is sent back to the cell stack with the help of pumps, which regulate the electrolyte's mass flow for recirculation and maintain a flow rate that clears any gas bubbles adhering to the electrodes. Dukic and Fitak's research highlighted the advantages of forced over natural convection, particularly in terms of the electrolyser's voltage-current characteristics (Đukić and Firak, 2011).

These pumps also manage the electrolyte's flow rate to dissipate heat in subsequent stages. Temperature regulation of the circulating electrolyte is managed through heat exchangers and

controllers, typically maintaining a constant temperature around 70°C. Excessive heat, generated by the electrolysis process at higher voltages, can accelerate corrosion and compromise gas purity due to increased gas molecule diffusion through the diaphragm (Diéguez et al., 2008).

Before re-entering the cell stack, the electrolyte passes through an agitation tank, essential due to disparity in the half-cells' gas output and water consumption, although it may lead to increased gas impurity (Haug et al., 2017). Post-separation, the hydrogen stream is cooled in a tower setup consisting of a heat exchanger and a demister, followed by a separator to remove moisture, ensuring high-quality hydrogen gas. The hydrogen gas undergoes moisture removal, temporary storage, and subsequent purification in deoxidizer. It is then thoroughly dried in adsorber columns to achieve 99.999% purity before compression for storage (Tjarks et al., 2018).

3.3. Impurities in product gases

The presence of impurities in the product gases H_2 and O_2 during the alkaline electrolysis is influenced by several factors related to electrolysis process like electrolyte carryover, electrode material degradation, Gas crossover and contaminants in the feed water. Tiny droplets of the electrolyte solution usually in KOH can be carried along with gas bubbles during electrolysis, which leads presence of KOH the hydrogen and oxygen.

Although alkaline electrolyzes are designed to minimize gas crossover, small amounts of H_2 can diffuse into the O_2 side and vice versa. This can be resulted in the presence of oxygen in the hydrogen stream and hydrogen in the oxygen stream. The gas crossover takes place because of two phenomena 1) gas dissolution in the electrolyte and 2) diffusion through the separator.

3.3.1. Gas solubility in alkaline electrolysis

Haug et al., (2017) proposed to quantitatively estimate dissolved gas content under electrolysis conditions. They leveraged the Setchenov relation, a well-established principle describing the inverse relationship between gas solubility (C_{is}) and salt concentration (Cs). This relation, expressed logarithmically, sheds light on how electrolyte concentration affects gas solubility relative to pure water solubility (C_{io}) (Ruetschi and Amlie, 1966),

The Setchenov relation equation

$$log \frac{C_{io}}{C_{is}} = K C_s \quad (8)$$

$$K = (\sum h_i - h_{Gi}) n_i \quad (9)$$

Incorporates the Setchenov constant (K), which integrates salt-specific constants (h_i) and gas-specific constants (h_{Gi}). Notably, (h_{Gi}) encompasses the temperature-dependent behavior of gas solubility, ensuring robust estimations across relevant temperature ranges for electrolysis. n_i represent ion index, multiplication salt and gas specific gas constants.

Figure 7 compares the gas solubilities in relation to potassium hydroxide concentration in models and measurements. Haug et al., (2017) verified the calculated solubilities shown in Figure 7 reveals that as the concentration of electrolyte increases the gas solubility decreases.

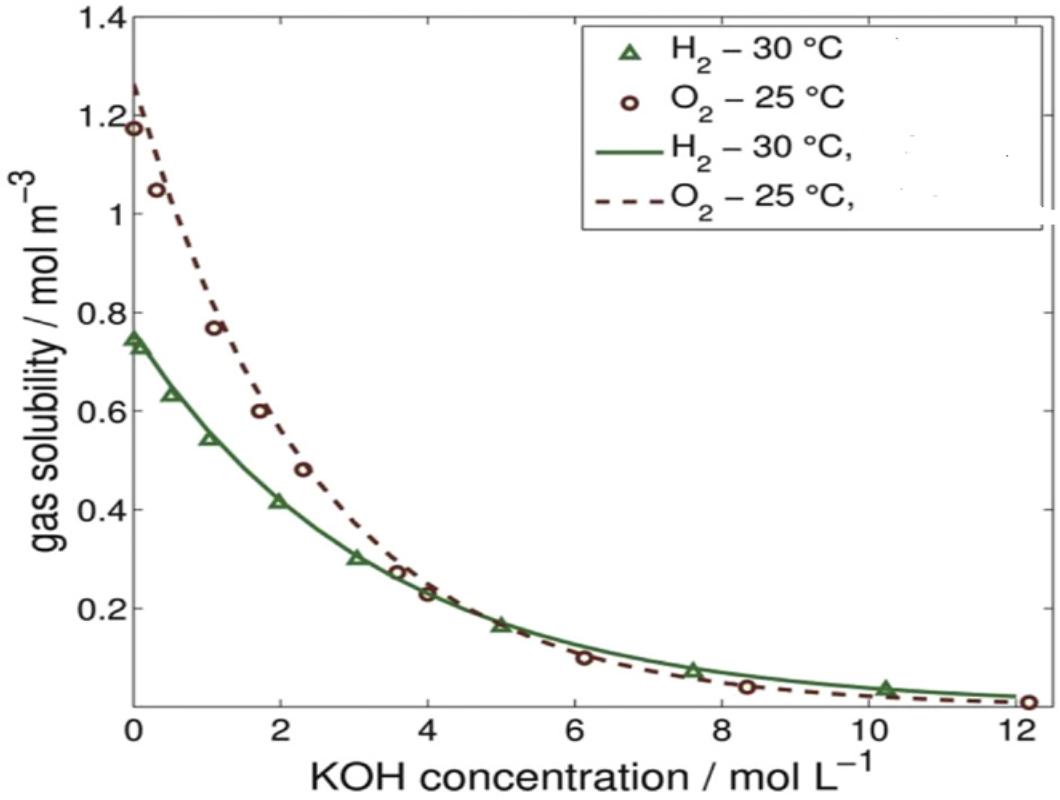

Figure 7 comparison of the gas solubilities in relation to potassium hydroxide concentration in models and measurements (Haug et al., 2017).

Figure 8 reveals that the diffusion coefficients of product gases within electrolyte solute decreases. Higher temperature led to decrease in the solubility resulting a reduction of gas impurities.

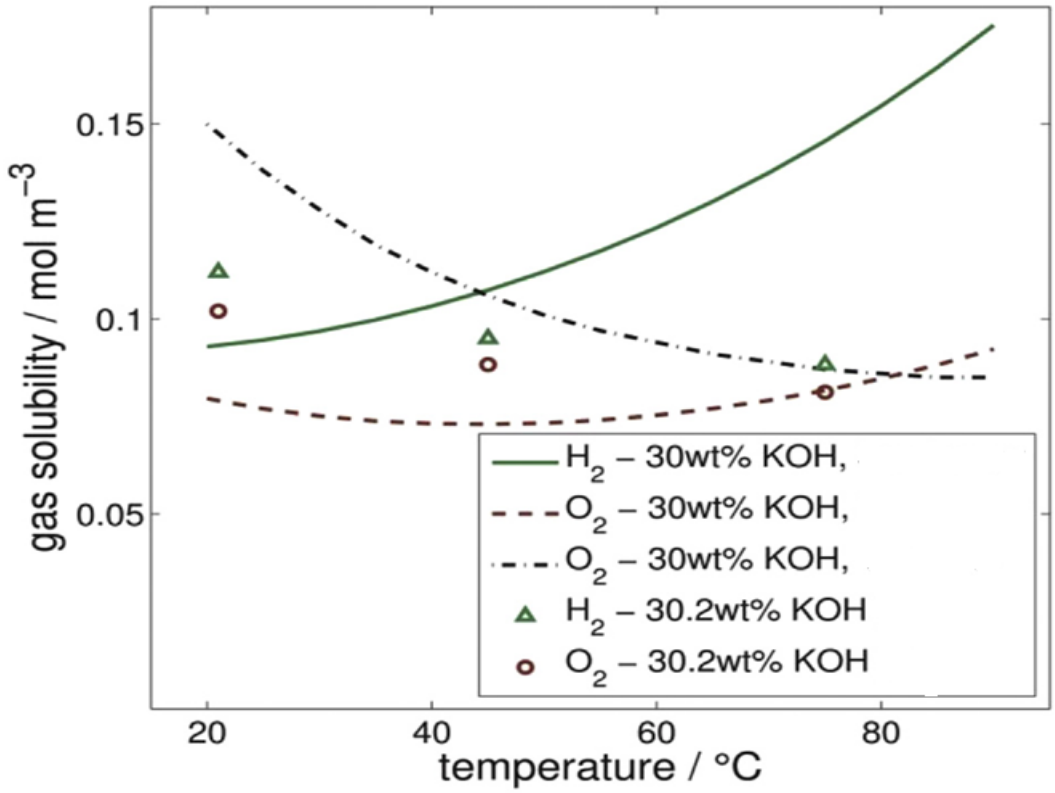

Figure 8 Comparison of the solubilities of H_2 and O_2 in relation to temperature in models and measurements at 30 and 30.2 wt% KOH (Hauge et al., 2017).

3.3.2. Diffusion through separator

In an electrolysis cell, the separator serves two purposes: it prevents the mixing of H_2 and O_2 gases and avoids short circuits between the electrodes. To minimize voltage drops, the separator must be conductive to OH^- ions and stable in highly alkaline environments. The porosity and tortuosity of the separator influence its conductivity, as current flows through the liquid electrolyte within its pores. The gases in the other half-cell can be contaminated by dissolved gases in the electrolyte that permeate through the separator. Increasing electrolyte flow rates can reduce this diffusion. Gas crossover is often described using Fick's law, which is commonly applied in both PEM and alkaline electrolysis models.

$$N_{i,\ cross} = \frac{\varepsilon D_{i,j} A E_c}{\tau \delta_{sep}} (C_i^{cat} - C_i^{an}) \quad (10)$$

Where A represents the separator area n denotes the number of cells, δ_{sep} represents the separator thickness, ε describes the porosity of the separator, and τ indicates tortuosity, and $D_{i,\ j}$ is the diffusion coefficient. For instance, the porosity of AGFA's commercially available Zirfon$_{TM}$ Perl UTP 500 separator is 0.5 ± 0.1 and its thickness is 500 ± 50 µm (Haug et al., 2017). Tortuosity values vary from 2 to 7, while detailed data on its tortuosity are not available (Landesfeind et al., 2016). The Figure 9 represent H_2 and O_2 diffusion coefficients. As concentration rises, the diffusion coefficients of oxygen and hydrogen both decreases. The diffusion coefficients improve with rising temperatures, and it has a more effect on hydrogen diffusion coefficients than on oxygen diffusion coefficients.

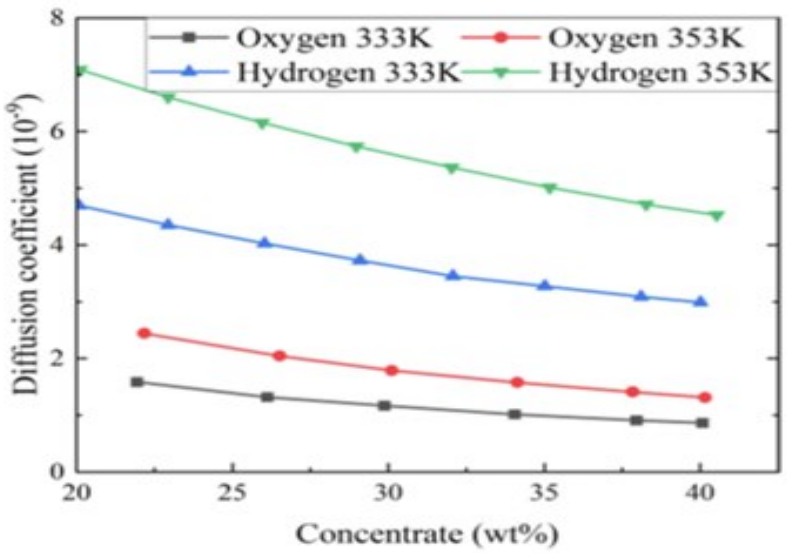

Figure 9 Temperature and concentration of KOH solution affect the diffusion coefficients of oxygen and hydrogen (Hu et al., 2022)

4. Safety limits and operational range

4.1. Safety limits

The issue of gas purity in AWEs is a significant concern due to the potential for O_2 and H_2 to mix because of gas diffusion and electrolyte circulation (Trinke et al., 2018). This is particularly critical when the volume fraction of HTO surpasses 4%, posing a risk of creating

an explosive gas mixture that can severely compromise the safety of the system. For safety reasons, the system is required to shut down when the HTO exceeds 2% volume fraction.

Gas purity in AWEs is closely linked to their operational conditions before undergoing any purification processes, the production of pure H_2 through AWEs under high load conditions is 99.9% pure by volume, while the oxygen purity ranges between 99.0% and 99.5% (Trinke et al., 2018). However, during low load operations, gas purity tends to decline, increasing the likelihood of surpassing the explosive safety threshold. This issue becomes more pronounced at higher gas pressures within the electrolyser as shown in the Figure 10. For example, at low pressure and low current density the HTO can reach 2% volume fraction safety limit. Whereas increase pressure at 100% and current density by 50% the HTO reaches 2.5% which importantly exceeding the safety limit leads to explosion.

This reduction in gas purity at low loads restricts the operational range of AWEs and poses a challenge for their integration with RES, which is emphasized by wide-ranging power fluctuations. Consequently, ensuring gas purity is another critical safety issue for higher production rate of H_2.

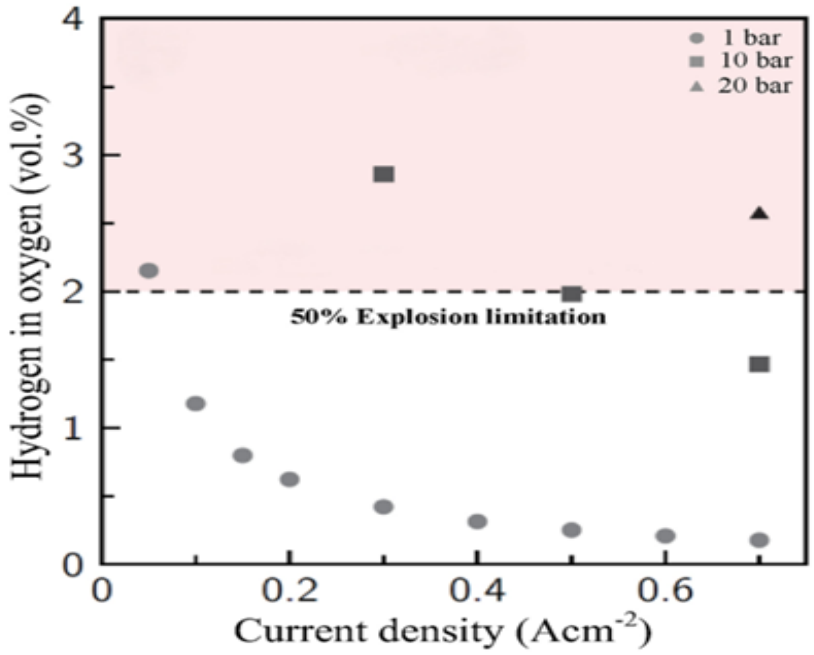

Figure 10 HTO with wide range of operating conditions

4.2. Operational range in alkaline electrolysis

In addition to safety issues, the consequences of product gases H_2 and O_2 which are soluble in the electrolyte diffused through the separator may cause decrease in the system efficiency duo to be increasing contamination from external gases. The characteristics of the separator influence this diffusive flux. By adjusting the physical parameters of separator there may be chance of decreasing the diffusive flux shown in the Eq(10) (Brauns et al., 2021).

The KOH electrolyte solution along with H_2 and O_2 mixture exit the stack and enter the individual gas separators and liquid pumped back to the electrolysis cell after separation has some dissolved gases in solution which needs to separate to increase the efficiency. Research indicates that electrolyte cycle splitting and mixing significantly affects gas impurity (Trinke et al., 2018). Gas contamination is lower in split electrolyte cycles since only dissolved product gas species reach the mixing point, unlike mixed electrolyte cycle operations.

The electrolyte has its influence on molar flux of mixing, which should be optimized. It needs to be high enough to dissipate heat produced by the electrochemical reaction's voltage losses without overheating the cell's constituent parts (Brauns et al., 2021). By splitting the flow rate of electrolyte concentration at given current the flow rates of mixing can decrease and swich between the flow modes for a particular time mixing can be handled these two strategies for minimising gas impurity. The electrolyte volume flow rate to reduce mixing molar flow concentration at the applied current density and alternating between flow modes to remove mixing molar flow for a predetermined period of time are two strategies for minimizing gas impurity.

4.3. Methods to prevent the gas accumulation in alkaline electrolysis

The presence of impurities in the gas produced by alkaline water electrolysis can be reduced by two methods: first one is optimization electrolyte recirculation, and second one is separation of dissolved gases from the electrolyte remove through the gas-liquid membrane separators.

4.3.1. Optimization of electrolyte recirculation

The gases which are dissolved in KOH solution will possibly pollute when it occurs to pass through the diaphragm which generated at the electrodes, this is known diffusion in electrolysis cell. Due to formation of Due to formation of nucleation bubbles, the electrolyte flow rates may decrease the diffusion by increasing its nucleation bubbles, the electrolyte flow rates may decrease the diffusion by increasing it (Tanaka et al., 2003). Moreover, the behavior observed in experiments conducted by Haug et al., (2017) studies demonstrate the importance of electrolyte flow rate in regulating gas purity. The results of their investigations, which were carried out at 80 °C and 31.7 wt% KOH concentration, showed that a decrease in product gas quality was caused by manipulating the electrolyte flow rate. More specifically, H_2 concentration dropped from 1.636 vol% to 0.701 vol% when flow rate was reduced from 100% to 20% at a current density of 0.5 kA m ^{2}. In the Figure 11 and Figure 12 it can be observed the same the gases from separator which soluble in KOH solution at higher flow rates. While considering the possibility of an increase in electrode bubble coverage, which could raise voltage of cell, maintaining an ideal electrolyte flow rate is essential to maintaining an optimum cell temperature. In terms of Faraday efficiency, a lower flow rate might not be optimal, but increased gas impurity can cause hydrogen to leak out along with the evolved oxygen. Moreover, additional hydrogen is lost during regeneration as a result of the OTH flow undergoing catalytic deoxygenation and drying (Smolinka et al., 2015). A thorough comprehension of the origins of impurities is necessary to maximize gas purity in alkaline water electrolysis procedures.

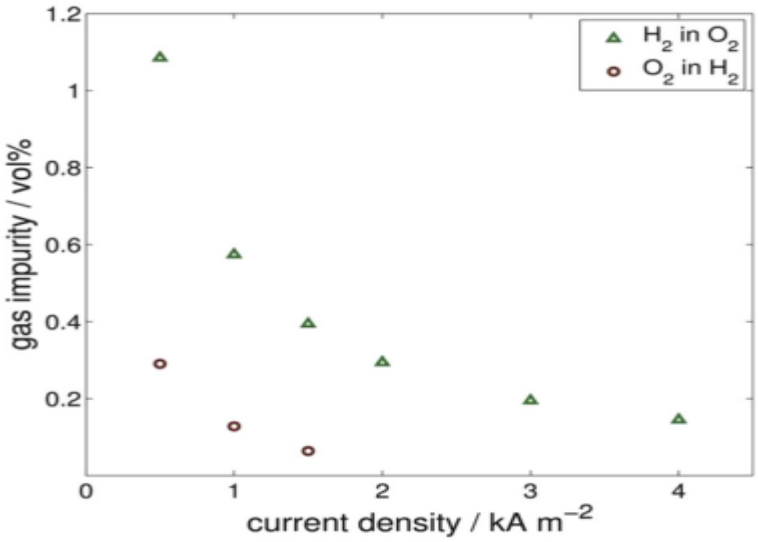

Figure 11 measuring the foreign gas content, both anodic and cathodic, in relation to current density. Operating parameters include mixed electrolyte cycles, T 80 ºC, KOH 31.2 wt%, and mean VL 0.33 L min^{-1}(Haug et al., 2017).

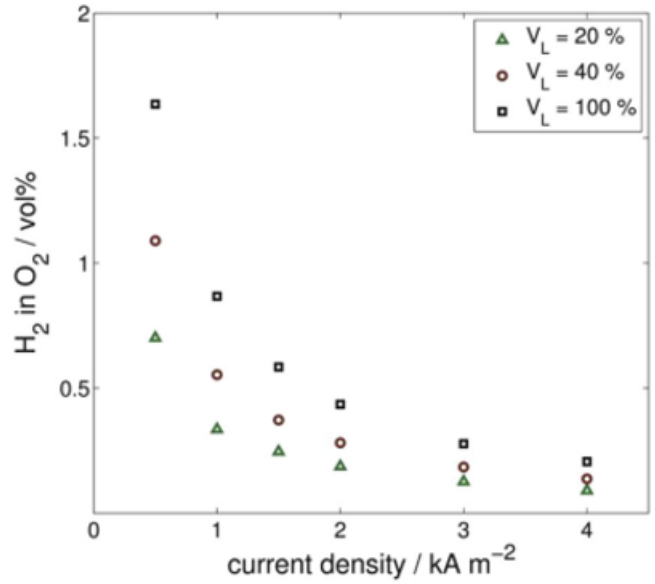

Figure 12 Anodic hydrogen content in relation to electrolyte flow rate and current density. Operating parameters include mixed electrolyte cycles, T 80 ºC, and KOH 31.7 wt% (Haug et al., 2017).

4.3.2. Dissolved gases separation

The process of membrane degassing effectively extracts (or incorporates) dissolved gases into) liquids. In the last 25 years, these membrane devices have replaced more antiquated technology including oxygen scavengers, forced draft deaerators, and vacuum towers. Typically, there are numerous uses for extracting H_2S from wastewater (Agrahari et al., 2013), O_2, and CO_2 from water (Tan et al., 2005). In a similar vein, oxidizing agents are required for the removal of soluble gases in a traditional way, including H_2S, O_2, and CO_2. However, the alternative approach, which uses dissolved gases from water in membrane contactors, avoids the well-known disadvantages of high energy needs, costly reagent and waste expenses, and generation of undesirable final products. (NH_3), (O_2), (CO_2), and H_2S are among the water-dissolved gases that the hollow fiber membrane effectively removes (Semmens et al., 1990).

Due to gas cross-over at the stack H_2 and O_2 at anode and cathode separation, there is now very little of these gases dissolved in the electrolyte solution that is cycled back into the electrolysis stack in alkaline electrolysis. The stack efficiency is influenced duo to the presence of these dissolved gases in the in-electrolyte solution. The relatively recent hollow fiber membrane contactors are recommended to eliminate these gases from membrane contactors. The hydrophobic or hydrophilic membranes are woven into hollow fibers and covered in a shell. The contact between two water phases is facilitated by the gas-liquid interface that is formed at both ends of the pore apertures. Without mixing or wetting the membrane material, gas desorption from one phase enters the hollow fibers and is taken up by the opposing phase (snow, 2024).

The purging gas or vacuum carries the dissolved gas molecules away. As a result, the gases are efficiently extracted from the liquid phase and concentrated inside the membrane module. As needed, the collected gases can be treated further or disposed of. In the meantime, the membrane module's degassed liquid emerges with lower dissolved gas concentrations.

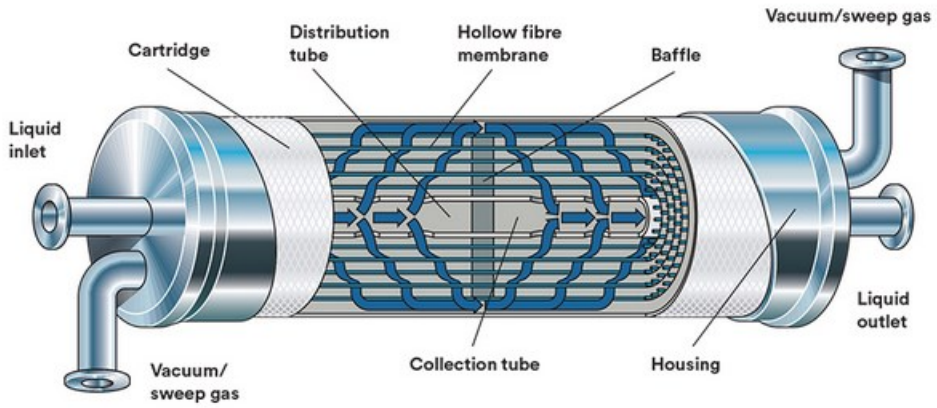

Figure 13 Hollow fibre membrane contactor for dissolved gas removal (snow, 2024).

5. Modelling of alkaline electrolysis

Modeling an electrolytic process involves creating a comprehensive framework with a process model and a cell model. The process model outlines mass and energy balances between different units, ensuring all inputs, outputs, and transfers are accurately accounted for. This provides a macroscopic view of the system, showing how components interact.

The cell model delves into the electrochemical operation of individual units, detailing current densities, potentials (electric potential differences driving reactions), efficiencies, and the electric power consumed by each unit. This provides a microscopic perspective complementing the process model.

The operational range of the electrolyser, defining safe and efficient functioning limits, is influenced by safety considerations and overall power efficiency. Safety issues are paramount to prevent accidents and equipment damage, setting strict operational limits.

5.1. Stack models

The reactions for anode and cathode in AWE as follows

$$Cathode: 2\,H_2O\ +\ 2e^-\ \rightarrow\ H_2 +\ 2OH^-\ E^o\ =\ 0.8280\,V \qquad (11)$$

$$Anode: 2OH^-\ \rightarrow\ 0.5\,O^2 +\ H^2O\ +\ 2e^-\quad E°\ =\ +0.4011\,V \qquad (12)$$

$$Overall\ reaction: H_2O\ \rightarrow\ H_2\ +\ 0.5\,O_2\quad E°\ =\ 1.2291\,V \qquad (13)$$

At the anode mole balance equations are:

$$\frac{d\dot{n}_{H_2O}}{dt} =\ \dot{n}_{H_2O}^{in}\ -\ \dot{n}_{H_2O}^{out}\ -\ \dot{n}_{H_2O}^{gen} \qquad (14)$$

$$\frac{d\dot{n}_{O_2}}{dt} =\ \dot{n}_{2OH^-}^{in}\ -\ \dot{n}_{O_2}^{out}\ -\ \dot{n}_{O_2}^{gen} \qquad (15)$$

where $\dot{n}_{2OH^-}^{in}$, $\dot{n}_{H_2O}^{in}$,$\dot{n}_{O_2}^{out}$, and $\dot{n}_{H_2O}^{out}$ are represented as anode molar flow rates of oxygen and water inlet and outlet $\dot{n}_{O_2}^{gen}$, $\dot{n}_{H_2O}^{gen}$, are the generation molar flow.

From the Eq(12) at the anode Faraday Law

$$\dot{n}_{H_2O}^{gen}\ =\ I/(2F) \qquad (16)$$

$$\dot{n}_{O_2}^{gen}\ =\ I/(4F) \qquad (17)$$

Where for 1 mole of electron transfer (½) mole of H2O and (¼) mole of O_2 are formed. F represent the faraday constant, and I denote current consumed.

$$I =\ i.A_e \qquad (18)$$

Where i represent current density and A_e denoted the electrode surface area

$$\dot{n}_{H_2O}^{gen} = \frac{\dot{n}_{H_2O}^{gen}}{A_e}\ =\ \frac{I}{(2A_eF)} = \frac{i}{2F} \qquad (19)$$

mole balance at cathode

$$\frac{d\dot{n}_{H_2O}}{dt} = \dot{n}_{H_2O}^{in} - \dot{n}_{H_2O}^{out} - \dot{n}_{H_2O}^{gen} \quad (20)$$

$$\frac{d\dot{n}_{H_2}}{dt} = \dot{n}_{H_2}^{in} - \dot{n}_{H_2}^{out} - \dot{n}_{H_2}^{gen} \quad (21)$$

From the reaction (11)

$$\dot{n}_{H_2}^{gen} = \frac{I}{2F} \quad (22)$$

Molar flux of H_2 can be written as

$$\dot{n}_{H_2}^{gen} = \frac{\dot{n}_{H_2}^{gen}}{A_e} = \frac{i}{2F} \quad (23)$$

5.1.1. Voltage overpotential

The overpotentials needed to overcome the activation energies of H_2 and O_2 production processes occurring on the surfaces of electrodes which are the source of reaction resistances. These overpotentials, which reflect the intrinsic energy barriers of the reactions and have an impact on the kinetics of the electrochemical processes, directly contribute to an increase in the total cell potential. These resistances, which are also known as overpotentials, are a natural byproduct of electrochemical reactions and are reliant on the electrodes' surface activity. Both R_{anode} and $R_{cathode}$ represent reaction resistances.

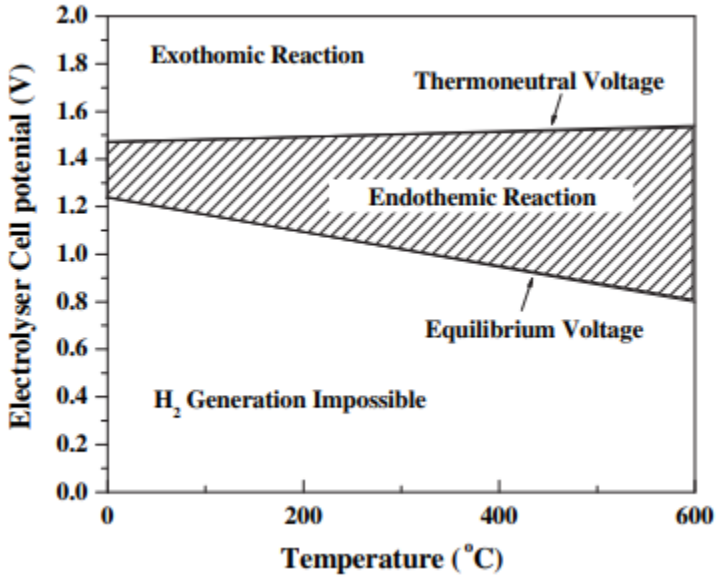

Figure 14 The production of H_2 through water electrolysis in relation with temperature potentials (Abdin et al., 2017).

Figure 14 The production of H_2 through water electrolysis in relation with temperature potentials The feasibility studies by Kai and Dongke, (2010) indicate the voltage range at which the hydrogen evolution reaction may be sustained at a particular temperature. The graph was divided into three sections by the voltage line of the equilibrium and the voltage line of the thermo-neutral. The voltage of equilibrium represents the lowest required theoretical potential for electrolysis-induced dissociation of water. There is no water electrolysis below this threshold. The thermo-neutral voltage denotes the lowest practicable voltage necessary for electrolysis. Electrolysis is endothermic below this voltage and exothermic beyond it (Kai and Dongke, 2010).

$$V = V_{oc} + V_{act} + V_{con} + V_{ohm} \tag{24}$$

V_{oc} = Open circuit voltage (It is ideal thermodynamic voltage which circuit should possess)
V_{act} = Activation energy overpotential for the reaction to take place
V_{con} = Overpotential due to concentration polarization (internal resistance)
V_{ohm} = External Circuit Overpotential (due to external resistance)

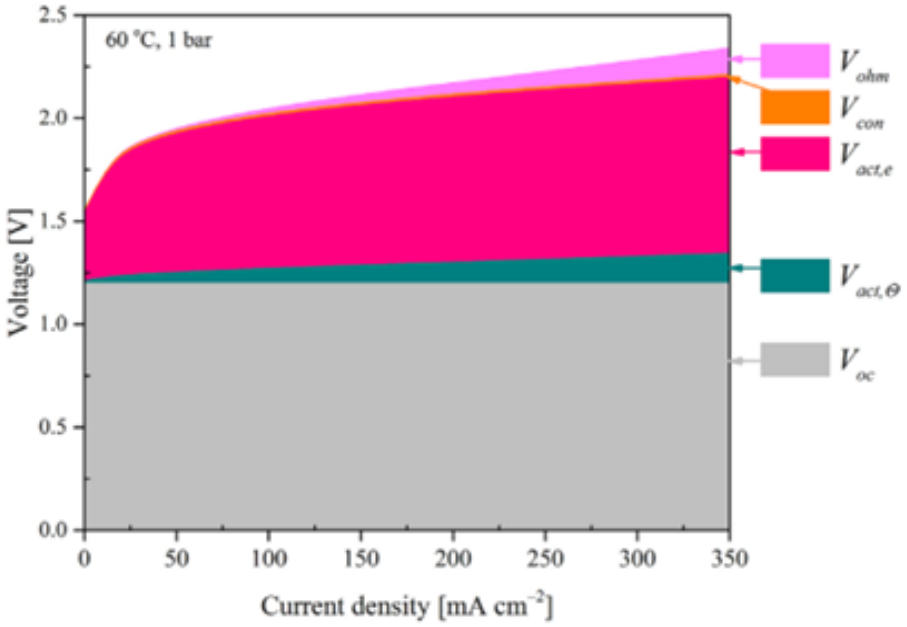

Figure 15 Overpotential terms contribution to the polarisation curve, V_{act} represents the bubble coverage contribution of the electrodes, while $V_{act\text{-}e}$, represents the bubble-free contribution of the electrodes (Abdin et al., 2017).

$$V_{oc} = E^{o}_{std} + \left(T - T_{ref}\right)\left(\frac{\Delta S^{\circ}}{2F}\right) + \left(\frac{RT}{2F}\right) ln\left(p_{H_2}\left(p_{O_2}\right)^{0.5}\right) \quad (25)$$

The extra potential is needed to an electrochemical cell to propel variables, including the kinetics of reaction, the electrode surface and material characteristics might affect the activation overpotential. Because it directly impacts the efficiency of energy and the devices performance, activation overpotential minimization is required in the design of efficient electrochemical systems, such as batteries, fuel cells, and electrolysers.

$$V^{an}_{act} = \frac{RT}{\alpha_{an}F} ln\left(\frac{i}{i^{an}_{o}}\right)\left(\frac{1}{[1-\Theta_{an}]}\right) \quad (26)$$

$$V^{cat}_{act} = \frac{RT}{\alpha_{cat}F} ln\left(\frac{i}{i^{cat}_{o}}\right)\left(\frac{1}{[1-\Theta_{cat}]}\right) \quad (27)$$

empirical expression for bubble coverage that takes temperature and current density into account and has been modified to take pressure effects into account (Hammoudi et al., 2012). where i_{lim} typically has a value of 300 kAm^{-2}

$$\Theta = \left[-97.25 + 182\frac{T}{T_{ref}}, -84\left(\frac{T}{T_{ref}}\right)^2\right]\frac{i}{i_{lim}}0.3\left[\frac{P}{P-P^{sat}_{H_2O,koh}}T\right] \quad (28)$$

The fluctuation in reactant concentration induced by continuing electrochemical reactions close to the electrode surface gives rise to a concentration or diffusion overpotential. It is widely ac

$$V_{con} = \left(\frac{RT}{4F}\right) ln\left(\frac{C^{O2-in}_{an}}{C^{O2-out}_{an}}\right) + \left(\frac{RT}{2F}\right) ln\left(\frac{C^{H2-in}_{cat}}{C^{H2-out}_{cat}}\right) \quad (29)$$

$$V_{ohm} = I\,R_{cell}\,(R_e + R_{el} + R_s) \quad (30)$$

Here R_{cell} represent the cell ohmic resistance, R_e denotes the resistance of electrode, R_{el} refers to the resistance of electrolyte, and R_s is the resistance of separator.

5.2. Process models

5.2.1. Mass balance

The overall AWE mass balance of the system can be described as the change of mass rate in time. This is determined by the difference between the inlet and outlet electrolyte flow $\dot{m}_{el,i}$ and $\dot{m}_{el,j}$ sum of reaction rate r_s.

$$\frac{d\dot{m}}{dt} = \sum\dot{m}_{el,i} - (\sum\dot{m}_{el,j} + \sum r_s) \quad (31)$$

The mass balance of cell of the electrolyte stack with in the cell is represented by Eq(66). Estimated mass flow on both electrode side shown in below equations where $\dot{m}^{con}_{H_2O}$ consumption of water, $\dot{m}^{pro}_{H_2O}$ is production of water, $\dot{m}_{H_2}$ is hydrogen production, $\dot{m}_{O_2}$ is oxygen production and E_c represent the total number of cells.

$$\frac{d\dot{m}}{dt} = \left(\dot{m}_{cat,i} + \dot{m}_{an,i}\right) - \left(\dot{m}_{cat,j} + \dot{m}_{an,j}\right) \quad (32)$$

$$\dot{m}_{cat,i} = \frac{\sum \dot{m}_{el,i}}{2E_c} \quad (33)$$

$$\dot{m}_{an,i} = \frac{\sum \dot{m}_{el,\ i}}{2E_c} \quad (34)$$

$$\dot{m}_{cat,j} = \dot{m}_{cat,i} + \dot{m}_{H_2} - \dot{m}_{H_2O}^{con} \quad (35)$$

$$\dot{m}_{an,j} = \dot{m}_{an,i} + \dot{m}_{O_2} + \dot{m}_{H_2O}^{pro} \quad (36)$$

5.2.2. Energy balance

A lumped-capacitance model is employed to easy the intricate differential heat equations needed to evaluate thermal systems such as electrolyser stacks. The continuous interaction RES and the AWE electrolyser result in the generation of heat that accumulates within system (Barco-Burgos et al., 2020). AWE electrolysis is greatly impacted by this heat in every way. It raises the diaphragm's and electrolyte's conductivity. However, it decreases electrode conductivity, which has a more influence on the current density and hydrogen production of the electrolytic cell (Vermeiren et al., 1996).

$$C\frac{dT}{dt} = \left(Q_{loss} - Q_{liq} - Q_{amb}\right) \quad (37)$$

The electrolyser temperature rate change over a time the material stack thickness is represented by $\frac{dT}{dt}$. Heat generated in relation to heat losses is represented by Q_{loss}. It decreases efficiency as voltage rises. As a result, the waste heat produced can be represented as follows:

$$Q_{loss} = E_c\left(U_{cell} - U_{pt}^{tn}\right)I \quad (38)$$

The term Q_{liq} represents the heat which is taken from the stack This liquid entering it is cooled by heat exchangers of electrodes. The heat removal process is needed to maintain the operating

temperature of the electrolyser stack there by ensuring efficient electrolysis. The expression can be detailed as

$$Q_{liq} = \dot{m}_{el,i}\, C_{P,el}\, (T_{stack} - T_{el,i}) \tag{39}$$

$\dot{m}_{el,i}$ *is* the rate of electrolyte mass flow. The specific heat capacity of the electrolyte is denoted by $C_{P,el}$, the temperature of the stack is T_{stack}, and the temperature of the electrolyte denoted by $T_{el,i}$.

The capacitance of heat in the order of the entire electrolyser stack, C_t is relation to density, heat capacity, and volume of elements that makes up a single electrolyser cell (Diéguez et al., 2008).

$$C_t = \left(\sum \rho_i C_{P_i} V_i\right) E_c \tag{40}$$

$$C_t = \left(\rho_{bi} C_{P_{bi}} V_{bi} + \rho_{mem} C_{P_{mem}} V_{mem} + 2\rho_{el} C_{P_{el}} V_{el}\right) E_c \tag{41}$$

5.2.3. Gas-liquid separation

The electrolyser stack produces bubbles containing hydrogen and oxygen, which are released along with electrolyte mixture. The separator is combined with a heat exchanger and a demister to enhance the separation process. The main tenets of this model are that liquid particles are spherical, that gas and liquid phases maintain height equilibrium, that the electrolyte density doesn't change, and that the mass change rate inside the vessel stays constant over time because of makeup water being periodically fed into the system. mass balance in the vessel used for the hydrogen-liquid separation.

$$\frac{d\dot{m}}{dt} = \sum \dot{m}_i - \sum \dot{m}_j \tag{42}$$

$$\sum \dot{m}_{\,i} = \dot{m}_{H_2,i} + \dot{m}_{el,i} + \dot{m}_{m,i} \tag{43}$$

$$\sum \dot{m}_j = (\dot{m}_{H_2,i}\, n_s + \dot{m}_{el,i}\,(1 - n_{sl})) + (\dot{m}_{el,i}\, n_{sl} + \dot{m}_{H_2,i}\,(1 - n_s) + \dot{m}_{m,i} \quad (44)$$

Where,

$\dot{m}_i$ and $\dot{m}_j$ is total inlet and outlet mass flow represented in Eq(47) and Eq(48),

$\dot{m}_{m,i}$ is the make–up feed water,

And n_s and n_{sl} is gas and liquid separation efficiencies respectively.

Eq(48) consists of two components that describe the flow dynamics within the gas-liquid separation vessel. The first component estimates the flow leaving outlet above the vessel. This flow comprises H_2 bubbles, and a small amount of electrolyte carried upward as moisture. The separation efficiency effectively how much of these components are separated from the electrolyte. The second component of the equation addresses the flow below. The efficiency of separation affects this flow as well, ensuring that the electrolyte, hydrogen, and impurities are appropriately managed and directed back into the system. The make-up feedwater flow depends upon the how much electrolyte is consumed in the electrolyser stack, $\dot{m}_{H_2,\ c}$ to form the end-product gas, as well as the amount of electrolyte dragged upward, $\dot{m}_{el,j,\ H_2up}$, $\dot{m}_{el,j,\ O_2up}$ in the gas-liquid separators to the O_2 and H_2 side.

$$\dot{m}_{m,i} = \dot{m}_{H_2,c} + \dot{m}_{el,j,\ H_2up} + \dot{m}_{el,j,O_2up} \quad (45)$$

5.2.4. Energy balance at the hydrogen-liquid separation vessel

The method employs to describe the balance of energy and thermal behavior is the lumped capacitance in the separator. The Eq(50) is used to explain the parameters in energy balance. Moreover, the energy balance of stack is closely relatable to even separation vessel. Thermal loss to the surrounding air is measured using the free convection of separator. Finally, the first law of thermodynamics is applied to assess the thermal colling effects, including those from the introduction of cold makeup water

$$C_{t,sep}\,\frac{dT}{dt} = -Q_{amb} - Q_{sensible} - Q_{cool} \quad (46)$$

5.2.5. Energy and mass balance at the oxygen-liquid separation vessel

The balance of mass and energy of O2-liquid separator vessel and the hydrogen-liquid separation vessel are derived using identical equations; the make-up feed's impact is not included in the equivalency.

5.2.6. Deoxidizer

$$2H_2^+\ (g) + O_2^-\ (g) \rightarrow 2H_2O\ (g) + 244.9\ kJ\ mol^{-1} \tag{47}$$

Purification of the hydrogen in the final stage of alkaline electrolysis process in the deoxidizer the where the oxygen and hydrogen reacts back to form moisture such that removal all oxygen present in the hydrogen product gas as impurity shown in the Eq(51).
According to experiment conducted by (Briguglio et al., 2019) in a packed bed reactor a alloy of cobalt and platinum can effectively and rapidly convert up to 4% of oxygen impurities in hydrogen into water.
The mass balance it mathematically presented as follows:

$$\frac{\mathrm{d\dot{m}}}{\mathrm{dt}} = \sum \rho_{\mathrm{i}} V_{\mathrm{i}} - (\sum \rho_{\mathrm{j}} V_{\mathrm{j}} + \sum r_{\mathrm{s}}) \tag{48}$$

$$\frac{d\dot{\mathrm{m}}}{dt} = (\dot{\mathrm{m}}_{H_2,i} + \dot{\mathrm{m}}_{O_2,i}) - (\dot{\mathrm{m}}_{H_2,pure} + \dot{\mathrm{m}}_{r,H_2O}) \tag{49}$$

where $\dot{\mathrm{m}}_{\mathrm{r,\,H_2O}}$ is the water generated during the reaction $\dot{\mathrm{m}}_{\mathrm{H_2,pure}}$ is the pure hydrogen outlet flow of the reactor. Finally, gas Flow enters the H_2-liquid separator, where the produced moisture is reduced to acceptable level, after it is passing through the deoxidizer.

5.3. Aspen library models for alkaline electrolysis

5.3.1. NRTL model 1

Sanchez et al., (2020) introduced a model for an alkaline electrolysis plant, which includes both the stack (where the actual electrolysis happens) and the other parts of the system needed for its operation, used Aspen plus for modeling. Since Aspen Plus lacks tools for modeling electrolysis cells, they used Aspen bespoke Modeler to construct a bespoke model for the stack. Equations describing significant variables such as voltage, efficiency, and gas purity depending on the current flowing through the system form the basis of this model.

For the additional components of the electrolysis plant, including pumps and heat exchangers, standard units available within the software were utilized. Simulations were conducted to assess the overall system performance and identify potential improvements. The results indicated that system performance enhanced by increasing the temperature and reducing the pressure. This modeling approach aids in evaluating the costs and benefits of AWE systems, especially when combined with industrial processes.

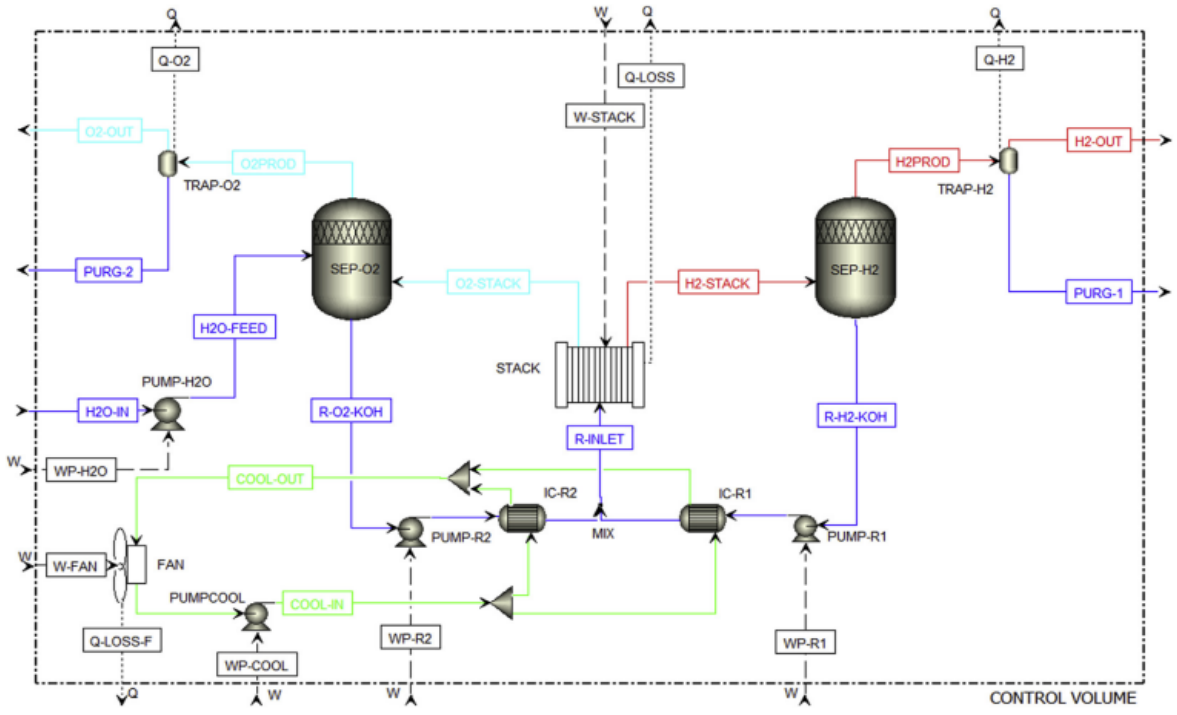

Figure 16 Aspen Plus process flow diagram of an alkaline electrolysis plant (Sanchez et al., 2020).

Aspen Plus doesn't have a built-in feature for modeling alkaline electrolysis cell stacks. So, in this study, they added a model for an AWE stack with the help of ACM. With ACM, you can create custom units for specific purposes. They used this tool to combined electrolysis cell process, allowing them to simulate the entire system.

To get started, they needed to create an Aspen Properties file. This file helps define the components of the system and select the property method to use. In their case, they chose a model called NRTL (Non-Random Two-Liquid) for their simulations. Then, they wrote down all the equations using the ACM language. This step is crucial because it ensures that the system has no unknowns and clearly defines what information goes in and out of the model. In this model, the interactions between molecules are accounted for through parameters that represent the non-randomness of mixing. These parameters are typically determined empirically through experimental data or theoretical calculations.

5.3.2. ENRTL-RK model 2

The example model is taken from in built model in aspen for alkaline electrolysis ("Aspen Technology," 2022), it is NEL A3880 electrolyser using the built-in electrolyser model in Aspen Plus. NEL A3880 has a net production rate of 5180-8374 kg/24h with 3.8-4.4 kWh/Nm3 power consumption per stack under ambient temperature (5-35 ºC). Further, the hydrogen purity can reach 99.9% or higher with an integrated hydrogen separator tank. Detailed specifications of NEL A3880 can be found in ("NEL," 2018).

utilizes the ENRTL-RK property method to characterize the behavior of both individual components and mixtures within the electrolyte system. For lighter gases such as O_2, H_2, and N_2, the Henry method is employed. The model defines the solution chemistry through the equilibrium between H_2O, OH^-, H_3O^+, and the dissociation of KOH into OH^- and K^+.

Within the Specification area, users can input various parameters including the power/current directed to the electrolyser, the tally of stacks and cells per stack within the device, as well as the operating temperature or duty. The model also accounts for the pressure drop occurring inside the electrolyser this model utilizes default values from (Abdin et al., 2017).

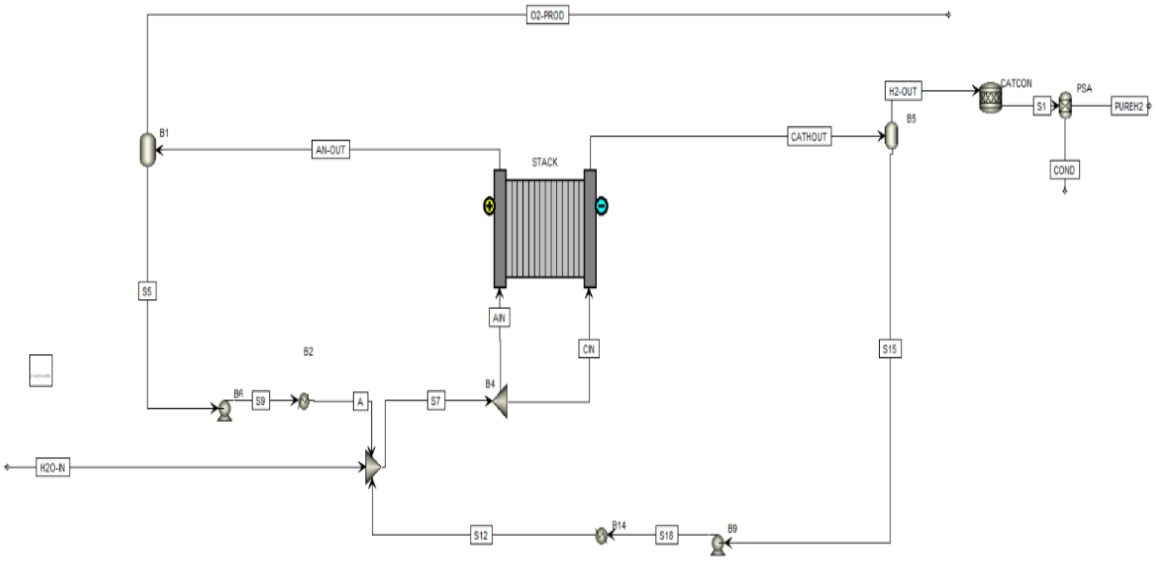

Figure 17 Aspen plus flow sheet of industrial alkaline electrolyser ("Aspen Technology," 2022)

The Aspen Plus model for an industrial-scale alkaline electrolyser is depicted in Figure 17, highlighting the electrolyser (labelled STACK) as the central component. The water from both electrodes is collected, recycled, and reintroduced into the electrolyser along with a new supply of water (H2O-IN). The outputs from the electrolyser are directed to Flash2 separators, which are responsible for extracting gases from the water; the water is then recirculated. To ensure the H_2 production stream (H2-OUT) is devoid of oxygen, it is processed through a stoichiometric reactor (CATCON), where oxygen is completely converted to water. Finally, to achieve pure hydrogen, the stream undergoes purification in a component separator, referred to as the PSA unit.

6. Applied part

6.1. Objective

The aim of this study is to design a AWE process model in Aspen Plus to investigate the effect of partial power loading to mixing of product gases, i.e. to hydrogen and oxygen purity. It focuses on how process parameters affect gas impurities, like hydrogen in oxygen (HTO) and oxygen in hydrogen (OTH). Additionally, the study examines how the removal of dissolved gases (H_2 and O_2) in electrolyte recirculation influences gas mixing.

6.2. Overall system description

The Figure 18. proposed system is simulated using Aspen Plus software. Multiple sensitivity analyses and studies are performed to examine the performance of a system. The system input water enters at 16 bar pressure and 80°C, and the alkaline solution KOH at 30 wt% initially enters at 71.7 m^3/h. This mixture is fed to the stoichiometric reactor (AE) to convert water into H_2 and O_2 gases, resembling the actual electrolysis process conducted by (Sakas et al., 2022). Generally, the bipolar plate in the electrolysis stack operates such that hydrogen production occurs in one half-cell, while oxygen production occurs in the other half-cell. In this process, water is consumed at the cathode, and only half of the consumed water is formed at the anode. This indicates a considerable amount of water is missing from the system, which must be fed into the process to maintain the initial electrolyte concentration. The produced stream (ROUT) from the reactor is connected to a flash separator (FLASH7) to calculate the vapor volume fraction. The mixed stream of liquid and vapor from the (MIXER3) is then fed to the membrane separator, which acts as the Zirfon™ Perl UTP 500 diaphragm, to separate oxygen and hydrogen. These separated streams are connected to two flash separators (FLASH2 and FLASH3) to separate the electrolyte from the O2-STACK stream to the anode side and the H2-STACK stream to the cathode side.

Electrolyte recirculation is achieved by centrifugal pumps (PUMP2 and PUMP3), which control the electrolyte circulation rate and water feed rate to FLASH2. The water inlet feed replaces the missing amount of water using the design spec in Aspen, which only allows the

necessary amount of water to maintain the 30 wt% KOH concentration. Usually, electrolyte recirculation serves to remove and drag into the flow all gas bubbles formed on the electrolyser stack electrode. These bubbles generally block the active surface area of the electrode, hindering the splitting reaction and reducing the hydrogen production rate. The separated O2-STACK and H2-STACK in the flash separators contain hydrogen, oxygen, and water vapor on both the anode and cathode sides, which are sent to separators (FLASH4 and FLASH5) to remove the water vapor as an impurity. The product stream O2-F at the anode side has a minimal amount of H_2 as an impurity (HTO), and H2-F at the cathode side has O_2 as an impurity (OTH). These impurities are analyzed with sensitivity analysis in Aspen Plus simulation against the duty of the reactor, which is the capacity of the process. The observed analysis is discussed in the Results and Discussion section, detailing how these impurities (HTO and OTH) affect the operational parameters of alkaline electrolysis.

In the Aspen Plus simulation shown in the Figure 19, the separator (FLASH7) is used to separate vapor and liquid flow rates of the ROUT stream from reactor AE to calculate the vapor volume fraction using a calculator block. It is assumed that when water converted to 0.5 vapor volume fraction, the duty of the reactor reaches the maximum capacity of the process because the excessive vapor resists the conduction of electric current. The gas-liquid membrane separator MEMSEP1 (hollow fiber membrane separator) is used to remove the dissolved gases H_2 and O_2 in the electrolyte, which is recirculated from the anode and cathode of the electrolyte stack. Further purification of H_2 is achieved in the deoxidizer (DE-OXO), where most oxygen molecules react to produce H_2O, which is sent into Flash6 to separate the hydrogen gas as product gas feed to a compressor (COMPR).

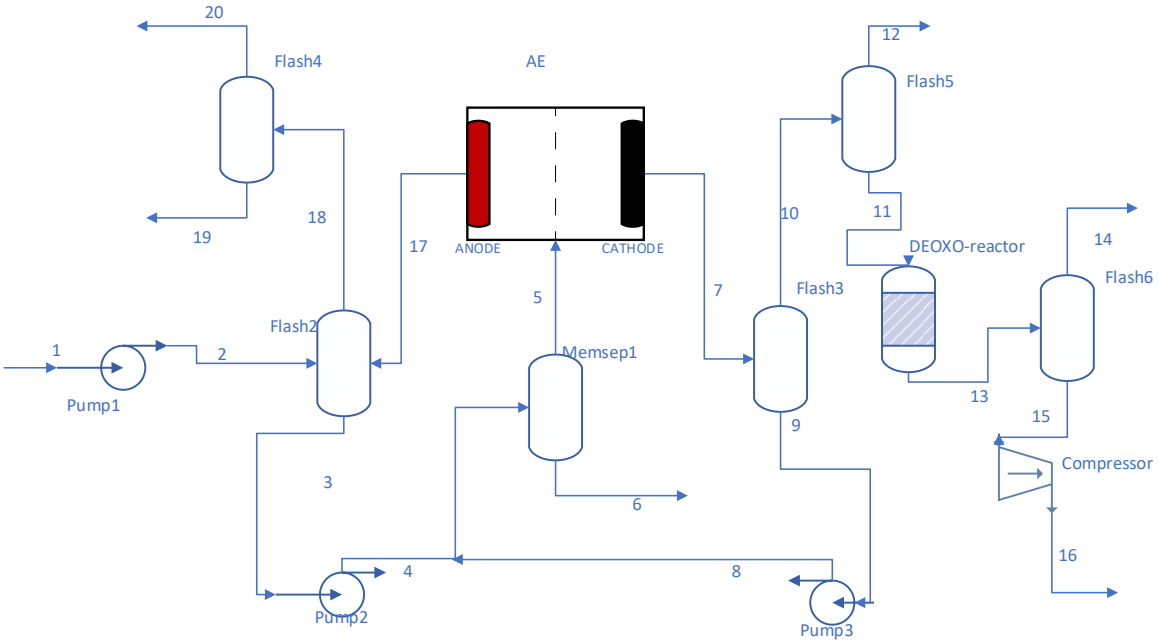

Figure 18 Process flow sheet diagram of alkaline water electrolysis at 71 m^3/h electrolyte circulating rate, 30 wt% KOH, 80 ºC and 16 bar.

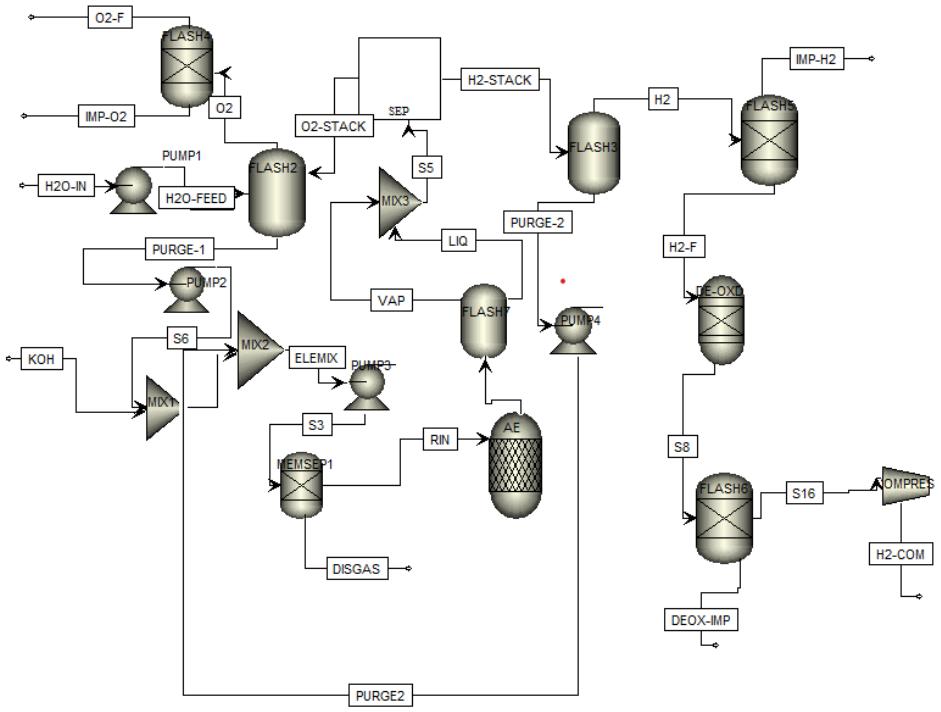

Figure 19 Aspen Plus flow sheet for alkaline electrolysis process at 71 m^3/h electrolyte circulating rate, 30 wt% KOH, 80 ºC and 16 bars.

6.3. Mass balance

Table 1 Mass balance table for alkaline water electrolysis given in mass balance data obtained from the Aspen Simulation the overall pure hydrogen production 63 kg/h at the maximum capacity 2.51 MW. The amount of duty required for pumps and compressor together is 50 KW. Overall, the inlet mass water feed 600.53 kg/h is equal to the outlet flow.

Table 1 Mass balance table for alkaline water electrolysis given in the Figure 19

	Temp °C	Pressure bar	Mass flow kg/h	Component flow kg/h			
				H_2	O_2	H_2O	KOH
H2O-IN	25	1	600.53	0	0	600.53	0
H2-FEED	80	16	600.53	0	0	600.53	0
O2-STACK	80	16	35914.6	0.32	507.041	24607.1	10800
H2-STACK	80	16	35477.8	64.3	5.84	24607.3	10800
PURGE-1	80	16	36011.6	0.0063	11.62	25200	10800
PURGE-2	80	16	35392.7	0.63	0.065	24592	10800
R-IN	80	16	71392	0.15	2.92	49791.8	21600
DISGAS	80	16	9.24	0.47	8.76	0	0
ELEMIX	80	16	71404	0.63	11.68	49791.9	21600
ROUT	80	16	71392	64.62	512.88	49214.3	21600
O2	80	16	503.27	0.312	498.42	7.52	0
H2	80	16	84.7	63.67	5.77	15.24	0
O2-F	80	16	498.7	0.312	498.42	0	0
H2-F	80	16	69.45	66.67	5.77	0	0
H2-IMP	80	16	15.24	0	0	15.24	0
O2-IMP	80	16	7.52	0	0	7.52	0
DEOOX-IMP	80	16	6.5	0	0	6.5	0
H2-COM	1052	50	63	63	0	0	0

7. Result and discussion

This section discusses the causes and effects of gas crossover in alkaline electrolysis and suggests methods to reduce it, along with the results of implementing these methods. Gas crossover, resulting in impurities of hydrogen in oxygen (HTO) and oxygen in hydrogen (OTH), occurs due to the dissolution of gas particles in the circulating electrolyte and their diffusion through the separator. A simulation of the alkaline electrolysis process Figure 20 shows that at the plant's maximum capacity of 2.54 MW, 69.2 kg/h of hydrogen is produced with 5.8 kg/h of oxygen as an impurity, and 507.4 kg/h of oxygen is produced with 0.312 kg/h of hydrogen as an impurity.

7.1. Dissolution of gas molecules in the circulating electrolyte

Usually, the dissolved gases in the circulating electrolyte can significantly affect the performance and safety of alkaline electrolysis, which affect the ionic conductivity lead to higher energy consumption for the same amount of hydrogen and oxygen production. The side reaction reactions oxygen impurity at the cathode and hydrogen impurity at anode can reduce the overall efficiency of the electrolysis. In the electrolyte circulation approximately 12.5 kg/h oxygen and hydrogen together are there. At first basic simulation in the Figure 20 studies the amount hydrogen (H_2) is produced with oxygen (O_2) as an impurity (OTH) and oxygen produced with hydrogen as an impurity (HTO), ensuring that the product stream of H_2 contains less than 4 mole% O_2 and vice versa. To achieve this, the study correlates variables such as capacity (MW), vapor fraction, and gas composition (HTO and OTH). At a vapor volume fraction of 0.5 and the maximum capacity of the plant is 2.54 MW, as shown in the Figure 21. The Figure 23 indicates that OTH values at different capacities are much smaller compared to HTO values, concluding that HTO is the most critical parameter for system operation at different capacities. For safe operation, even if the plant load drops by 47% to 1.2 MW from the maximum capacity of 2.54 MW, the HTO value does not reach 2 mole%, which is within safe operating conditions. Exceeding this level will trigger an automatic shutdown of the plant for safety.

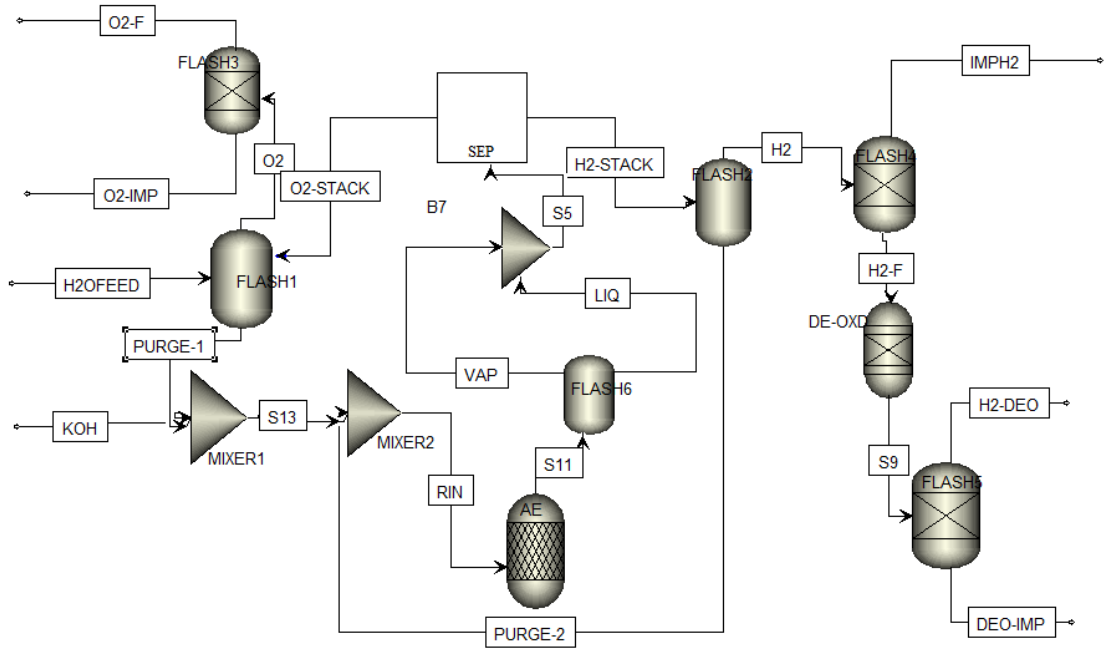

Figure 20 Simulation flow sheet in Aspen Plus to produce HTO and OTH values to compare load values at 71 m^3/h electrolyte circulating rate, 30 wt% KOH, 80 ºC and 16 bars.

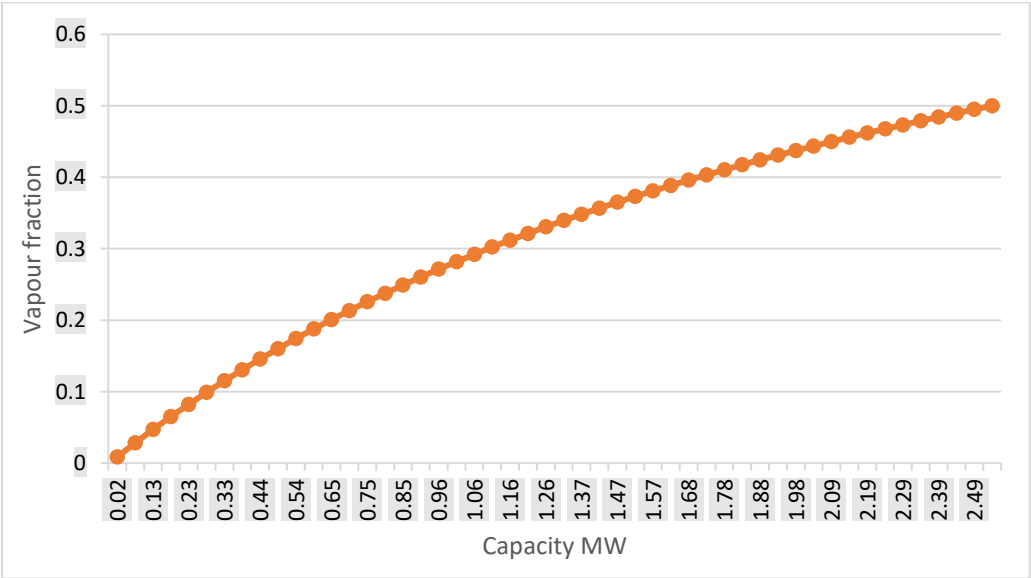

Figure 21 vapour fraction vs loading capacity at 71 m^3/h electrolyte circulating rate, 30 wt% KOH, 80 ºC and 16 bars.

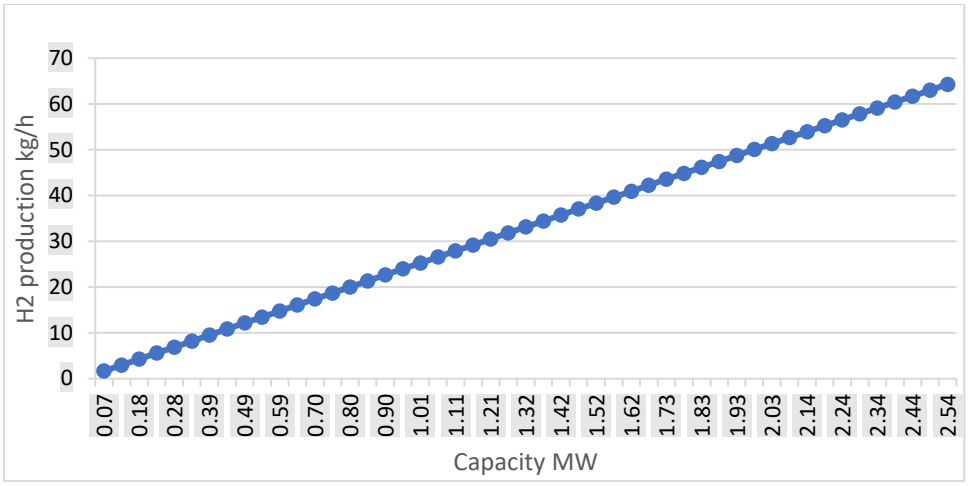

Figure 22 Production of Hydrogen kg/h at different loading capacities at 71 m^3/h electrolyte circulating rate, 30 wt% KOH, 80 ºC and 16 bars.

Figure 21 and Figure 22 illustrate the correlation between vapor volume fraction, and load capacity (MW) in hydrogen production. As the vapor volume fraction increases the reactor duty also increase, leading to higher hydrogen production. It is assumed that maximum electrolysis capacity is achieved resulting in a 0.5 vapor fraction. At this point, the reactor duty reaches its maximum capacity of 2.54 MW, as shown in the Figure 21. To estimate the effect of impurities (HTO in oxygen and OTH in hydrogen) on the electrolysis system, the product gases are analyzed. It is crucial to ensure that the hydrogen in oxygen and vice versa does not exceed 4%, to prevent the risk of explosion. For safety, the plant should shut down when the impurity mixture reaches 2%. The Figure 23 shows the gas composition (HTO and OTH) values at different loads. At maximum load, the impurities in the product gases are very low. However, as the load decreases, the impurities increase. At minimum load, impurities surpass the critical point. Among the impurities, HTO is the more critical parameter, reaching the critical point first. In conclusion, the plant operates safely until the load drops from 2.54 MW to 1.21 MW, which is 47% of the total load. Beyond this load, there is a risk of explosion due to the increased impurity levels.

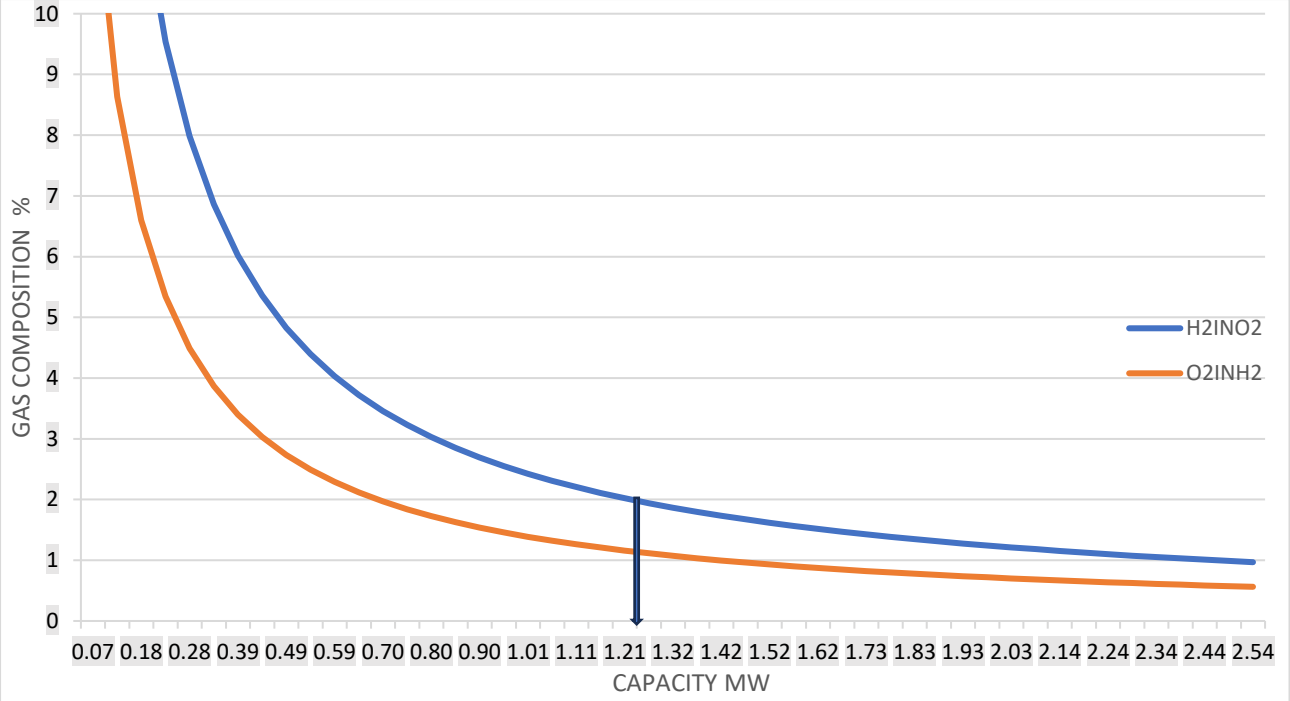

Figure 23 Comparison of amount impurities HTO and OTH at different capacities at 71 m^3/h electrolyte circulating rate, 30 wt% KOH, 80 ºC and 16 bars.

7.2. Diffusion through the separator

The hydrogen circulation rate can significantly impact the overall electrolyte composition and distribution within the electrolyser. Dissolved gases in the electrolyte can permeate through the separator to the anode side, leading to hydrogen crossover, which reduces purity and raises safety concerns. In the Table *2* below, the diffusion rate of hydrogen in the electrolyte through the diaphragm is calculated using the diffusion coefficient of hydrogen in the electrolyte, the porosity and tortuosity of the Zirfon™ Perl UTP 500 diaphragm (Haug et al., 2017), and the concentration gradient of the hydrogen Eq(10). The diffusion rate of hydrogen through the separator is 0.0135 kg/h. In the 72 m^3/h of total electrolyte circulation flow the concentration gradient of hydrogen 3.43 mol/m^3. The circulating rate of hydrogen in the electrolyte for 2 g/mol molar mass of hydrogen is 0.49 kg/h. Usually, a higher electrolyte circulation helps in quickly removing dissolved hydrogen from the vicinity of the cathode helps reducing the concentration gradient of hydrogen and removal of dissolved gases in the electrolyte through membrane separator will also help decrease in diffusivity and decrease the impurity level.

Table 2 calculation of Hydrogen diffusion rate through diaphragm.

Parameter	Value	Unit
Diffusion coefficient ($D_{H2,KOH}$)	5.63×10^{-9}	m^2/s
Diaphragm thickness (δ)	0.0005	m
Porosity (ε)	0.5	-
Tortuosity (τ)	4.5	-
Area of diaphragm (A)	2.66	m^2/s
Number of cells	326	-
Concentration gradient (C)	3.46	mol/m^3
Electrolyte flow rate	72	m^3/h
Concentration of H_2	3.46	mol/m^3
Circulating rate of H_2 in electrolyte	249.12	mol/h
Circulating rate of H_2 in electrolyte	0.49	kg/h
Diffusion rate of H_2 (N)	1.3×10^{-2}	kg/h

7.3. Methods to prevent gas mixing

7.3.1. Effect of pressure in oxygen separator

To decrease impurities, the pressure in the Flash2 separator was reduced from 16 bar to 1 bar. This adjustment led to a significant reduction in impurities in the hydrogen gas, more so than in the oxygen, due to the sudden change in pressure. As shown in the Figure 24 this pressure reduction caused the hydrogen gas impurities (OTH) to drop from approximately 22% to 1.5%. However, regarding safety concerns, the hydrogen impurity in oxygen (HTO) did not show a significant change. The system remains within the safe level of 2% hydrogen in oxygen at a 1.15 MW load, which is 46% of the maximum load of 2.49 MW. Without the pressure reduction, this safety threshold is at 1.2 MW, as shown in the Figure 23.

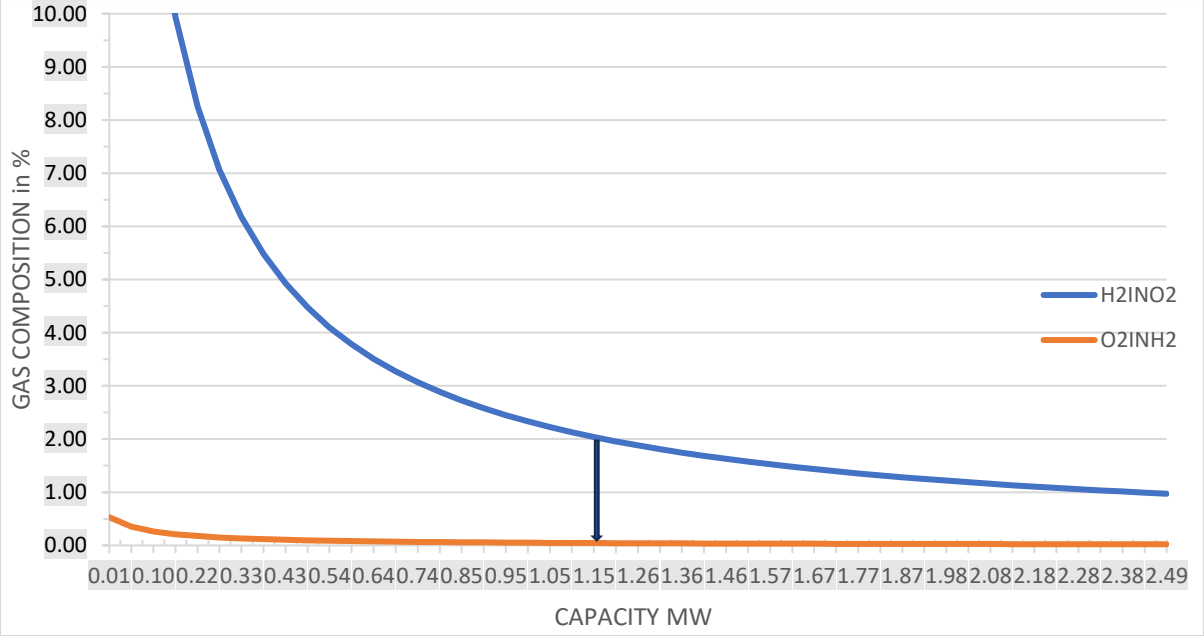

Figure 24 Effect of low pressure (1 bar) in oxygen separation tank on product gas composition at 71 m^3/h electrolyte circulating rate, 30 wt% KOH, 80 ºC and 16 bars.

7.3.2. Control of electrolyte circulation rate

The higher circulation rate of electrolyte helps in better heat dissipation, maintaining a stable operating temperature, which prevent overheating and reduce the need for additional cooling systems, that will potentially lowering power consumption. Ensures that the electrolyte is evenly distributed, maintaining uniform conductivity across the cell, which reduce the resistive losses and improve the efficiency of the electrolysis process. It also, helps in effectively removing gas bubbles from the electrode surfaces and electrolyte, which minimizes the blockage of active sites on the electrodes and reduces the resistance to ion flow, thus lowering the power load. In the Figure 26 it can be observed that as the electrolyte flow decreases the power load decreases but the level gas composition both HTO and OTH are constant can be seen in Figure 25. That means because of recirculation even if the load drops impurity level within the safety conditions.

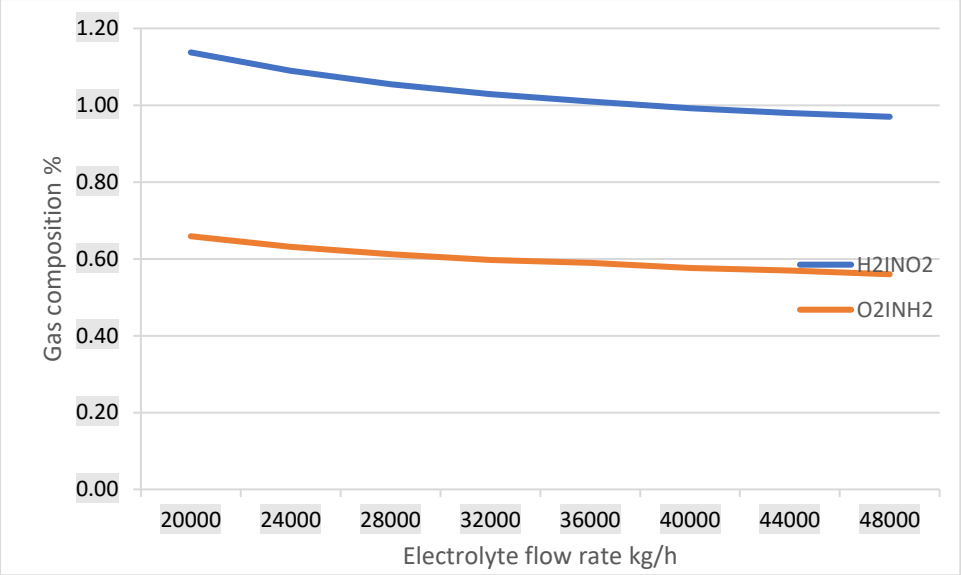

Figure 25 Effect of electrolyte circulation rate on product gas composition at 30 wt% KOH, 80 ºC and 16 bars.

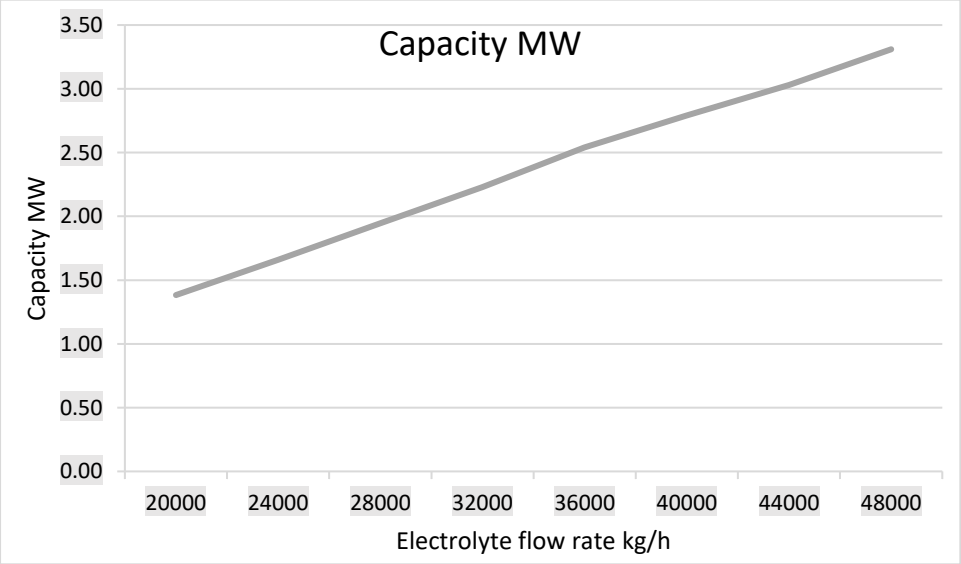

Figure 26 Power load at different electrolyte flowrates at 30 wt% KOH, 80 ºC and 16 bars.

7.3.3. Dissolved gases separation using membrane separation.

The gas transfer membrane is designed to remove gases from liquids, enabling direct contact between the gaseous phase and the aqueous stream without dispersion. A commercially available hollow fiber membrane with a capacity of 1.5 m^3/h is used to remove oxygen and hydrogen from a 30 wt% KOH electrolyte solution ("Tanal," 2024), which is recycled from both the anode and cathode of the electrolyte stack. Typically, water flows outside the

membrane fibers, while the inside of the hollow fibers is vacuum pumped, or gas purged. The membrane module is housed in a cylindrical tank with a diameter of 168 mm and a length of 1205 mm between the liquid inlet and outlet, featuring a DN32-tricamp port. The distance between the vacuum/sweep gas port (DN25-tricamp) and the inlet/outlet is 860 mm. The module is fabricated from modified polypropylene (PP) and contains fibers with an inner diameter of 0.22 mm, an outer diameter of 0.4 mm, and a pore size of 0.0001 mm. The standard removal rate for dissolved gases is 75-95%. The module can operate at temperatures between 5°C and 65°C, with a maximum feed temperature of 0.1 MPa, membrane pressure of 0.2 MPa, and a working pH range of 3-12. To treat the total feed containing dissolved hydrogen and oxygen gases, 61 of these membrane contactor modules are required.

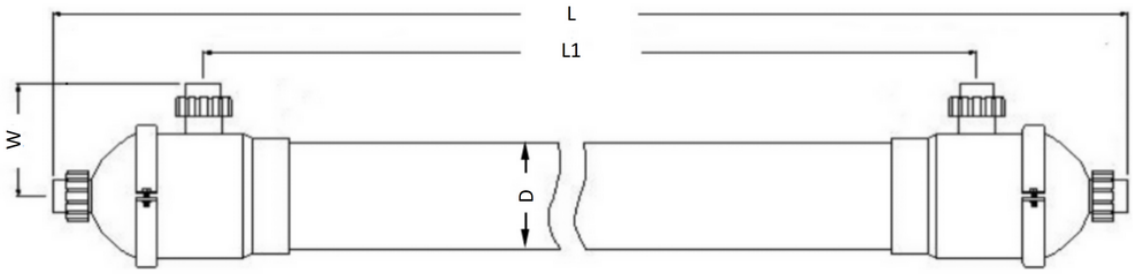

Figure 27 Hollow fibre membrane separator for dissolved gas separation

Table 3 Hollow fibre membrane separator model design specifications

Model	D mm	L mm	L1 mm	Pore size mm	Liquid port	Vaccum port	Capacity m^3/h	Total number of modules
MCO2	168	1205	860	0.0001	DN32 tri-clamp	DN25 tri-clamp	1.5	61

Capacity of module = 1.5 m^3/h

Total feed to treat = 71.3 m^3/h

Total number of modules = 48

The circulating rate of hydrogen in the electrolyte 0.49 kg/h from the Table 2. After the removal of 75% dissolved hydrogen in the hollow fiber membrane, the hydrogen is electrolyte circulation is 0.1242 kg/h. The diffusion rate around 10% of the circulation rate is significantly influencing the reduction of impurities. The Figure 29 presents a graph comparing the gas composition of HTO impurities against capacity (MW) for processes with and without the gas-liquid membrane separator. HTO impurities are identified as the most critical parameter for safety concerns compared to OTH impurities. The removal of dissolved gases enhances the purity of the product gases. The system maintains safety levels even if the load drops from the maximum capacity of 2.51 MW to 0.28 MW, which is approximately 11% of the maximum load. Without the removal of dissolved gases, this safety threshold is at 47%.

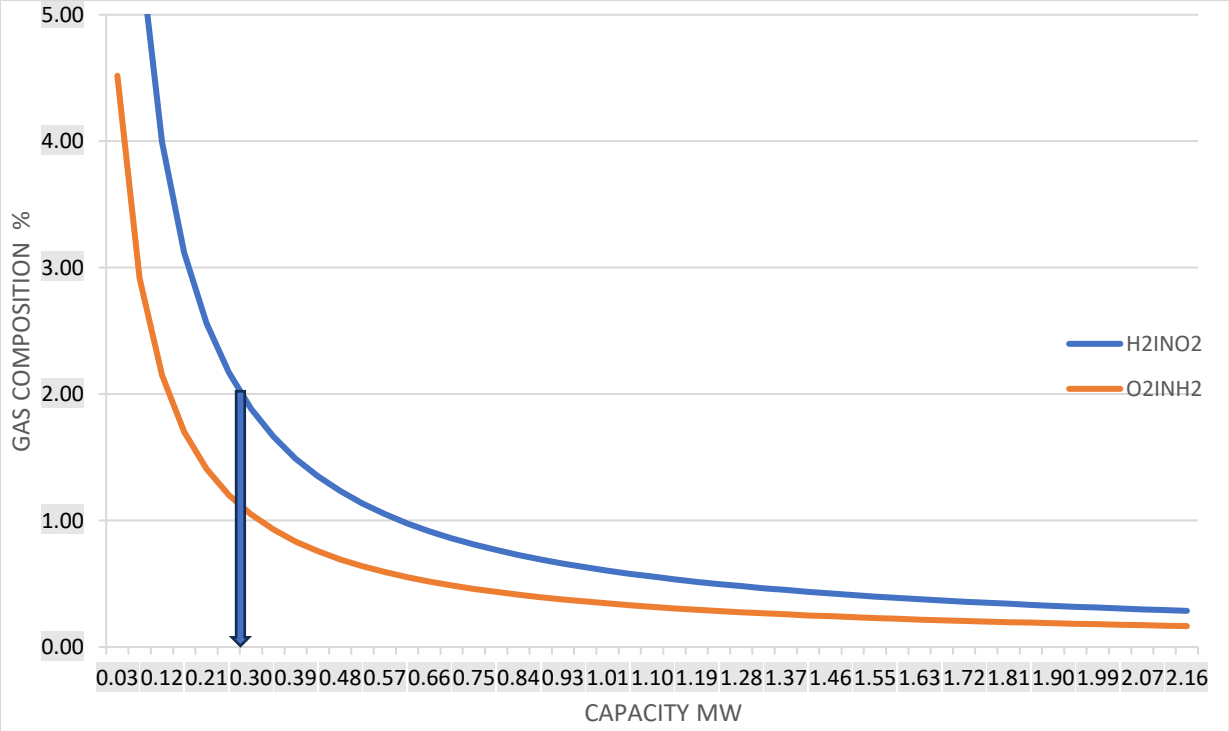

Figure 28 Effect of gas removal membrane on gas composition at 71 m^3/h electrolyte circulating rate, 30 wt% KOH, 80 ºC and 16 bars.

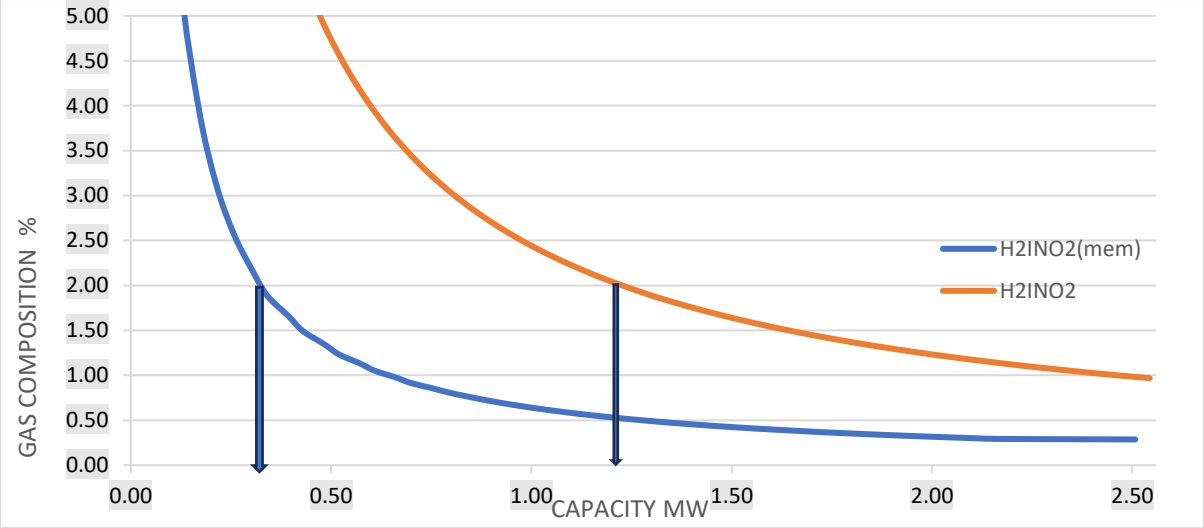

Figure 29 Comparison of oxygen gas composition with membrane and without membrane separation at 71 m^3/h electrolyte circulating rate, 30 wt% KOH, 80 °C and 16 bars.

The following Table 4 describes the amount of hydrogen lost in the process of producing pure hydrogen with membrane separator and without membrane separator. With membrane separator the total amount of hydrogen produced from the electrolysis stack is 65.13 kg/h. Some hydrogen is lost as impurities on the anode side in the oxygen, amounting to 0.47% or 0.312 kg/h. Additionally, 0.73% of hydrogen is lost in the membrane separator, dissolved in the electrolyte solution. Furthermore, hydrogen is lost in the deoxidizer, which is used to react hydrogen with oxygen to eliminate oxygen impurities, resulting in a 1.12% loss. The total amount of hydrogen lost in the process to produce pure hydrogen is 1.49%. Whereas in the process without membrane the total hydrogen production in the electrolysis stack is 65.26 kg/h. Hydrogen lost with oxygen gas 0.31 kg/h as impurity which is 0.48%. Additionally, hydrogen lost in the oxygen removal reactor is 0.73 kg/h and total amount of hydrogen in the process without membrane separator is 1.59% which means 1.04 kg/h. Overall with membrane separator total of loss of hydrogen is less compared to the process without membrane separator.

Table 4 Overall H_2 production and losses in the alkaline electrolysis process with membrane and without membrane separator at 71 m^3/h electrolyte circulation rate, 30 wt% KOH, 80 °C, and 16 bars.

	with membrane separator		without membrane separator	
Mass flow rate	kg/h	%	kg/h	%
Total H_2 production in reactor	65.13	100	65.26	100
H_2 lost in oxygen	0.31	0.48	0.31	0.48
H_2 lost in dissolved gas separation	0.48	0.74	0.00	0.00
H_2 lost in oxygen removal reactor	0.18	0.27	0.73	1.12
H_2 Total losses	0.97	1.49	1.04	1.59

8. Conclusions

In this study, a comprehensive AWE process model was developed using the Aspen Plus simulation environment. The primary focus was to analyze how load capacity variations in alkaline electrolysis impact the impurity composition in the product gases. The study particularly emphasized the challenges posed by variable nature of power inputs from renewable energy sources. These fluctuations can disrupt the power supply to the electrolysis process, complicating the maintenance of efficient hydrogen production and leading to increased gas crossover due to the dissolution of gas particles in the electrolyte and their diffusion through the separator.

Three methods were proposed to mitigate gas crossover: optimizing electrolyte circulation rates, adjusting pressure in the oxygen separator, and using hollow fiber membrane separators to remove dissolved gas impurities. The simulation results demonstrated significant improvements in reducing gas impurities with each method. For instance, the basic simulation indicated that at maximum capacity (2.54 MW), 63 kg/h of hydrogen is produced with impurity levels well within safe limits. Even with a 47% reduction in power load to 1.21 MW, impurities remained below the critical threshold.

The first method, reducing pressure in the oxygen separator, showed that impurities could be effectively managed in hydrogen gas, although there is not much effect on H_2inO_2 but we are

at safety level even when the power load dropped to 1.15 MW. The second method, varying electrolyte flow rates, resulted that even the load capacity increases with increasing flow rate the impurities are at constant level within safe limits across different flow rates. The third method, incorporating membrane separators, allowed for a substantial decrease in the power load limit, to 0.28 MW, 10% of the total load enhancing system safety and performance even with significant power fluctuations.

These findings underscore the importance of optimizing operating conditions, including electrolyte flow rates and load capacities, to maintain high purity levels in hydrogen and oxygen production while ensuring the safety and efficiency of the alkaline electrolysis process. The study also highlights the potential of using simulation models to predict and improve the operational range and safety of electrolysis systems under variable renewable energy inputs.

9. References

Abdin, Z., Webb, C.J., Gray, E.MacA., 2017. Modelling and simulation of an alkaline electrolyser cell. Energy 138, 316–331. https://doi.org/10.1016/j.energy.2017.07.053

Agrahari, G.K., Rawat, A., Verma, N., Bhattacharya, P.K., 2013. Removal of dissolved H2S from wastewater using hollow fiber membrane contactor: Experimental and mathematical analysis. Desalination 314, 34–42. https://doi.org/10.1016/j.desal.2012.12.027

Atmospheric Alkaline Electrolyser [WWW Document], 2018. . Nel Hydrog. URL https://nelhydrogen.com/product/atmospheric-alkaline-electrolyser-a-series/

Barco-Burgos, J., Eicker, U., Saldaña-Robles, N., Saldaña-Robles, A.L., Alcántar-Camarena, V., 2020. Thermal characterization of an alkaline electrolysis cell for hydrogen production at atmospheric pressure. Fuel 276, 117910. https://doi.org/10.1016/j.fuel.2020.117910

Brauns, J., Schönebeck, J., Kraglund, M.R., Aili, D., Hnát, J., Žitka, J., Mues, W., Jensen, J.O., Bouzek, K., Turek, T., 2021a. Evaluation of Diaphragms and Membranes as Separators for Alkaline Water Electrolysis. J. Electrochem. Soc. 168, 014510. https://doi.org/10.1149/1945-7111/abda57

Brauns, J., Schönebeck, J., Kraglund, M.R., Aili, D., Hnát, J., Žitka, J., Mues, W., Jensen, J.O., Bouzek, K., Turek, T., 2021b. Evaluation of Diaphragms and Membranes as Separators for Alkaline Water Electrolysis. J. Electrochem. Soc. 168, 014510. https://doi.org/10.1149/1945-7111/abda57

Brauns, Jörn., Turek, Thomas., 2020. Alkaline Water Electrolysis Powered by Renewable Energy: A Review. Processes 8, 248. https://doi.org/10.3390/pr8020248

Briguglio, N., Siracusano, S., Bonura, G., Sebastián, D., Aricò, A.S., 2019. Flammability reduction in a pressurised water electrolyser based on a thin polymer electrolyte membrane through a Pt-alloy catalytic approach. Appl. Catal. B Environ. 246, 254–265. https://doi.org/10.1016/j.apcatb.2018.12.079

Buttler, A., Spliethoff, H., Turek, 2018. Current status of water electrolysis for energy storage, grid balancing and sector coupling via power-to-gas and power-to-liquids: A review. Renew. Sustain. Energy Rev. 82, 2440–2454. https://doi.org/10.1016/j.rser.2017.09.003

Carmo, M., Fritz, D.L., Mergel, J., Stolten, D., 2013. A comprehensive review on PEM water electrolysis. Int. J. Hydrog. Energy 38, 4901–4934. https://doi.org/10.1016/j.ijhydene.2013.01.151

CGEP, 2024. Demystifying Electrolyzer Production Costs - Center on Global Energy Policy at Columbia University SIPA | CGEP % [WWW Document]. Cent. Glob. Energy Policy Columbia Univ. SIPA CGEP. URL https://www.energypolicy.columbia.edu/demystifying-electrolyzer-production-costs/

Cheng, H., Xia, Y., Wei, W., Yongzhi, Z., Bo, Z., Leiqi, Z., 2024. Safety and efficiency problems of hydrogen production from alkaline water electrolyzers driven by renewable energy sources. Int. J. Hydrog. Energy 54, 700–712. https://doi.org/10.1016/j.ijhydene.2023.08.324

David, M., Alvarez, H., Ocampo-Martinez, C., Sánchez-Peña, R., 2020. Dynamic modelling of alkaline self-pressurized electrolyzers: a phenomenological-based semiphysical approach. Int. J. Hydrog. Energy 45, 22394–22407. https://doi.org/10.1016/j.ijhydene.2020.06.038

Díaz-González, F., Sumper, A., Gomis-Bellmunt, O., Villafáfila-Robles, R., 2012. A review of energy storage technologies for wind power applications. Renew. Sustain. Energy Rev. 16, 2154–2171. https://doi.org/10.1016/j.rser.2012.01.029

Diéguez, P.M., Ursúa, A., Sanchis, P., Sopena, C., Guelbenzu, E., Gandía, L.M., 2008. Thermal performance of a commercial alkaline water electrolyzer: Experimental study and mathematical modeling. Int. J. Hydrog. Energy 33, 7338–7354. https://doi.org/10.1016/j.ijhydene.2008.09.051

Economical Equivalent to Membrane Module, Element and Filter Cartridge [WWW Document], 2024. . Tanal. URL https://www.tanalwater.com/ (accessed 6.5.24).

Feng, Q., Yuan, X., Liu, G., Wei, B., Zhang, Z., Li, H., Wang, H., 2017. A review of proton exchange membrane water electrolysis on degradation mechanisms and mitigation strategies. J. Power Sources 366, 33–55. https://doi.org/10.1016/j.jpowsour.2017.09.006

Hammoudi, M., Henao, C., Agbossou, K., Dubé, Y., Doumbia, M.L., 2012. New multi-physics approach for modelling and design of alkaline electrolyzers. Int. J. Hydrog. Energy, HYFUSEN 37, 13895–13913. https://doi.org/10.1016/j.ijhydene.2012.07.015

Haug, P., Koj, M., Turek, T., 2017a. Influence of process conditions on gas purity in alkaline water electrolysis. Int. J. Hydrog. Energy 42, 9406–9418. https://doi.org/10.1016/j.ijhydene.2016.12.111

Haug, P., Koj, M., Turek, T., 2017b. Influence of process conditions on gas purity in alkaline water electrolysis. Int. J. Hydrog. Energy 42, 9406–9418. https://doi.org/10.1016/j.ijhydene.2016.12.111

Hine, F., 1985. Electrode Processes and Electrochemical Engineering. Springer US, Boston, MA. https://doi.org/10.1007/978-1-4757-0109-8

Hu, S., Guo, B., Ding, S., Yang, F., Dang, J., Liu, B., Gu, J., Ma, J., Ouyang, M., 2022. A comprehensive review of alkaline water electrolysis mathematical modeling. Appl. Energy 327, 120099. https://doi.org/10.1016/j.apenergy.2022.120099

Janjua, M.B.I., LeRoy, R.L., 1985. Electrocatalyst performance in industrial water electrolysers. Int. J. Hydrog. Energy 10, 11–19. https://doi.org/10.1016/0360-3199(85)90130-2

Kai Zeng, Dongke Zhang, 2010. Recent progress in alkaline water electrolysis for hydrogen production and applications. Prog. Energy Combust. Sci. 36, 307–326. https://doi.org/10.1016/j.pecs.2009.11.002

Landesfeind, J., Hattendorff, J., Ehrl, A., Wall, W.A., Gasteiger, H.A., 2016. Tortuosity Determination of Battery Electrodes and Separators by Impedance Spectroscopy. J. Electrochem. Soc. 163, A1373. https://doi.org/10.1149/2.1141607jes

Leng, Y., Chen, G., Mendoza, A.J., Tighe, T.B., Hickner, M.A., Wang, C.-Y., 2012. Solid-State Water Electrolysis with an Alkaline Membrane. J. Am. Chem. Soc. 134, 9054–9057. https://doi.org/10.1021/ja302439z

LeRoy, R.L., 1983. Industrial water electrolysis: Present and future. Int. J. Hydrog. Energy 8, 401–417. https://doi.org/10.1016/0360-3199(83)90162-3

Manabe, A., Domon, H., Kosaka, J., Hashimoto, T., Okajima, T., Ohsaka, T., 2016. Study on Separator for Alkaline Water Electrolysis. J. Electrochem. Soc. 163, F3139. https://doi.org/10.1149/2.0191611jes

Meng, N., Michael K.H. Leung, Dennis Y.C. Leung, 2008. Technological development of hydrogen production by solid oxide electrolyzer cell (SOEC). Int. J. Hydrog. Energy 33, 2337–2354. https://doi.org/10.1016/j.ijhydene.2008.02.048

Momirlan, M., Veziroglu, T.N., 2005. The properties of hydrogen as fuel tomorrow in sustainable energy system for a cleaner planet. Int. J. Hydrog. Energy 30, 795–802. https://doi.org/10.1016/j.ijhydene.2004.10.011

O'Hayre, R., Cha, S.-W., Colella, W., Prinz, F.B., 2016. Fuel Cell Fundamentals. John Wiley & Sons.

Paidar, M., Fateev, V., Bouzek, K., 2016. Membrane electrolysis—History, current status and perspective. Electrochimica Acta 209, 737–756. https://doi.org/10.1016/j.electacta.2016.05.209

Parra, David., Patel, M.K., Parra, David., 2016. Techno-economic implications of the electrolyser technology and size for power-to-gas systems. Int. J. Hydrog. Energy 41, 3748–3761. https://doi.org/10.1016/j.ijhydene.2015.12.160

Peng, S., 2023. Alkaline Water Electrolysis, in: Peng, S. (Ed.), Electrochemical Hydrogen Production from Water Splitting: Basic, Materials and Progress. Springer Nature, Singapore, pp. 57–68. https://doi.org/10.1007/978-981-99-4468-2_3

Phillips, R., Dunnill, C.W., Vepsäläinen, 2016. Zero gap alkaline electrolysis cell design for renewable energy storage as hydrogen gas. RSC Adv. 6, 100643–100651. https://doi.org/10.1039/C6RA22242K

Rozain, C., Millet, P., 2014. Electrochemical characterization of Polymer Electrolyte Membrane Water Electrolysis Cells. Electrochimica Acta, Electrochemical Impedance Spectroscopy 131, 160–167. https://doi.org/10.1016/j.electacta.2014.01.099

Ruetschi, P., Amlie, R.F., 1966. Solubility of Hydrogen in Potassium Hydroxide and Sulfuric Acid. Salting-out and Hydration. J. Phys. Chem. 70, 718–723. https://doi.org/10.1021/j100875a018

Sakas, G., Ibáñez-Rioja, A., Ruuskanen, V., Kosonen, A., Ahola, J., Bergmann, O., 2022. Dynamic energy and mass balance model for an industrial alkaline water electrolyzer plant process. Int. J. Hydrog. Energy 47, 4328–4345. https://doi.org/10.1016/j.ijhydene.2021.11.126

Sanchez, M., Amores, E., Abad, D., Rodríguez, L., Clemente-Jul, C., 2020. Aspen Plus model of an alkaline electrolysis system for hydrogen production. Int. J. Hydrog. Energy 45, 3916–3929. https://doi.org/10.1016/j.ijhydene.2019.12.027

Sánchez, M., Amores, E., Rodríguez, L., Clemente-Jul, C., 2018. Semi-empirical model and experimental validation for the performance evaluation of a 15 kW alkaline water electrolyzer. Int. J. Hydrog. Energy 43, 20332–20345. https://doi.org/10.1016/j.ijhydene.2018.09.029

Schalenbach, M., Carmo, M., Fritz, D.L., Mergel, J., Stolten, D., 2013. Pressurized PEM water electrolysis: Efficiency and gas crossover. Int. J. Hydrog. Energy 38, 14921–14933. https://doi.org/10.1016/j.ijhydene.2013.09.013

Schröder, V., Emonts, B., Janßen, H., Schulze, H. -P., 2004. Explosion Limits of Hydrogen/Oxygen Mixtures at Initial Pressures up to 200 bar. Chem. Eng. Technol. 27, 847–851. https://doi.org/10.1002/ceat.200403174

Semmens, M.J., Foster, D.M., Cussler, E.L., 1990. Ammonia removal from water using microporous hollow fibers. J. Membr. Sci. 51, 127–140. https://doi.org/10.1016/S0376-7388(00)80897-2

Smolinka, T., Garche, J., Hebling, C., Ehret, O., 2011. Water electrolyzer for hydrogen storage systems – study on the state of the art of the technology and future development trends. Presented at the 6th International Renewable Energy Storage Conference and Exhibition.

Smolinka, T., Jürgen Garche, Emile Tabu Ojong, 2015. Hydrogen production from renewable energies - electrolyzer technologies [WWW Document]. URL https://publica.fraunhofer.de/entities/publication/85ddb855-011b-4bc7-9eee-3bb1441a8d8c/details (accessed 3.25.24).

snow, pure, 2024. Membrane Degassing Technology O2 and CO2 [WWW Document]. URL https://www.snowpure.com/technologies/membrane-degassing-technology-liqui-cel/ (accessed 5.28.24).

Souza, R.F. de, Padilha, J.C., Gonçalves, R.S., de Souza, M.O., Rault-Berthelot, J., 2007. Electrochemical hydrogen production from water electrolysis using ionic liquid as electrolytes: Towards the best device. J. Power Sources 164, 792–798. https://doi.org/10.1016/j.jpowsour.2006.11.049

Tan, X., Capar, G., Li, K., 2005. Analysis of dissolved oxygen removal in hollow fibre membrane modules: effect of water vapour. J. Membr. Sci. 251, 111–119. https://doi.org/10.1016/j.memsci.2004.11.005

Tanaka, Y., Uchinashi, S., Saihara, Y., Kikuchi, K., Okaya, T., Ogumi, Z., 2003. Dissolution of hydrogen and the ratio of the dissolved hydrogen content to the produced hydrogen in electrolyzed water using SPE water electrolyzer. Electrochimica Acta 48, 4013–4019. https://doi.org/10.1016/S0013-4686(03)00541-3

Tjarks, G., Gibelhaus, A., Lanzerath, F., Müller, M., Bardow, A., Stolten, D., 2018. Energetically-optimal PEM electrolyzer pressure in power-to-gas plants. Appl. Energy 218, 192–198. https://doi.org/10.1016/j.apenergy.2018.02.155

Trinke, P., Haug, P., Brauns, J., Bensmann, B., Hanke-Rauschenbach, R., Turek, T., 2018. Hydrogen Crossover in PEM and Alkaline Water Electrolysis: Mechanisms, Direct Comparison and Mitigation Strategies. J. Electrochem. Soc. 165, F502. https://doi.org/10.1149/2.0541807jes

Ulleberg, Ø., 2003. Modeling of advanced alkaline electrolyzers: a system simulation approach. Int. J. Hydrog. Energy 28, 21–33. https://doi.org/10.1016/S0360-3199(02)00033-2

Ursua, A., Barrios, E.L., Pascual, J., San Martín, I., Sanchis, P., 2016. Integration of commercial alkaline water electrolysers with renewable energies: Limitations and improvements. Int. J. Hydrog. Energy 41, 12852–12861. https://doi.org/10.1016/j.ijhydene.2016.06.071

Ursua, A., San Martín, I., Barrios, E.L., Sanchis, P., 2013. Stand-alone operation of an alkaline water electrolyser fed by wind and photovoltaic systems. Int. J. Hydrog. Energy 38, 14952–14967. https://doi.org/10.1016/j.ijhydene.2013.09.085

Vermeiren, Ph., Moreels, J.P., Leysen, R., 1996. Porosity in composite zirfon® membranes. J. Porous Mater. 3, 33–40. https://doi.org/10.1007/BF01135359

Xu, W., Scott, K., 2010. The effects of ionomer content on PEM water electrolyser membrane electrode assembly performance. Int. J. Hydrog. Energy, VIII symposium of the Mexican Hydrogen Society 35, 12029–12037. https://doi.org/10.1016/j.ijhydene.2010.08.055

Zarghami, A., Deen, N.G., Vreman, A.W., 2020. CFD modeling of multiphase flow in an alkaline water electrolyzer. Chem. Eng. Sci. 227, 115926. https://doi.org/10.1016/j.ces.2020.115926